BARIUM TITANATE SONAR TRANSDUCERS

Jack H. Conable

Letter on front cover:

BARIUM TITANATE SONAR TRANSDUCERS

JACK H. CONABLE

BARIUM TITANATE SONAR TRANSDUCERS

by

Jack Henry Conable

Lieutenant, United States Navy

Submitted in partial fulfillment
of the requirements
for the degree of
MASTER OF SCIENCE
IN
ENGINEERING ELECTRONICS

United States Naval Postgraduate School
Monterey, California

1 9 5 6

This work is accepted as fulfilling

the thesis requirements for the degree of

MASTER OF SCIENCE

IN

ENGINEERING ELECTRONICS

from the

United States Naval Postgraduate School

Prior to and during World War II, all of the material used in the construction of underwater ultrasonic transducers was of the magnetostrictive or single crystal piezoelectric type. During the war, E. Wainer and his associates at the Titanium Alloy Manufacturing Company discovered that certain titanates, barium titanate in particular, exhibited anomalous polarization effects. Further studies at the Laboratory for Insulation Research, M.I.T., established barium titanate as a new class of ferroelectric dielectrics. The polarized polycrystalline barium titanate showed certain analogies to ferromagnetic materials and also exhibited properties which usually had been associated with single piezoelectric crystals. Until this time the application of high power to ultrasonic transducers, of the piezoelectric type, had been limited by the delicate nature of the piezoelectric material and by the high voltages required. Quartz, for instance, is a good stable material, but it has a very high impedance, and is very expensive and difficult to produce in quantity. Rochelle Salt on the other hand has a low impedance, a low Q, but is relatively unstable and has definite temperature and humidity limitations. Thus barium titanate seemed to present a partial solution to these problems. It is relatively stable below 80°C, it has a low impedance, it is unaffected by humidity, and the basic material is relatively inexpensive as well as being available in great quantity.

This paper is divided into two major portions; the first dealing with electromechanical transducers, a discussion of barium titanate and its piezoelectric properties, and the fabrication of barium titanate

ceramics. The second section is devoted to the design and experimental results of a high resolution transducer employing barium titanate.

The author wishes to thank T. C. Madison of the General Electric Company for his assistance, encouragement, and cooperation in the preparation of this paper. He also wishes to express his gratitude to Professor Carl Menneken of the U. S. Naval Postgraduate School for introducing him to the field of barium titanate, and to Professor Lawrence E. Kinsler of the U. S. Naval Postgraduate School for introducing him to the field of ultrasonic transducers and his continued encouragement during the course of much of the work.

LIST OF ILLUSTRATIONS

LIST OF ILLUSTRATIONS

LIST OF ILLUSTRATIONS

Figure Page

CHAPTER I

INTRODUCTION

1. Fundamentals of Electromechanical Transducers

An Electromechanical Transducer is a device which is used to connect an electrical energy source to a mechanical energy load. If the device connects the energy source to the energy load without any transition or dissipation losses it is said to be an Ideal Transducer. To understand how electrical energy may be converted into mechanical energy it is necessary to investigate how the mechanical effects are created by electric and magnetic fields.

In an electric field, E, a force, F, is exerted on an electric charge, Q, such that; $F = QE$. This linear relationship between the force and applied electric field is valid for crystals of the piezoelectric family. The ratio between the force and the applied field is given by the piezoelectric coefficients which are determined by the electric asymmetry of the crystal. These piezoelectric coefficients vary for different types of crystals such as quartz, tourmaline, ADP (Ammonium dihydrogen phosphate), Rochelle Salt, and many others.

In the case of the magnetic field, we do not have a magnetic charge similar to the electric charge in an electric field, instead there is a current element, $I\ell$. The force exerted on this current element is proportional to the magnetic flux, B, such that; $F = BI\ell$. This is called the electrodynamic effect and makes possible the construction of electrodynamic transducers. If the flux is kept constant, by the application of a constant magnetic field, the exerted force will be proportional to the

amount of current applied and thus is also a linear relationship.

It is also possible to produce other electromechanical effects, which are applicable for transducer application, by the phenomena whereby the mechanical forces depend upon the square of an electric quantity. Examples being the force exerted on the plates of a charged condenser, the forces exerted by electrostriction, the force with which electric currents affect each other, the force of electromagnetic attraction, and the forces resulting from the magnetostrictive effect. Electrostriction is the behavior of certain materials by which they change their density and hence their dimensions when subjected to an applied electric field. Magnetostriction is the phenomenon by which certain metals and alloys such as nickel, colbalt, and permendur change their dimensions when subjected to a change in magnetizing force.

In order to approach the Ideal Electromechanical Transducer it is necessary to have a linear relationship between the electrical quantity and the mechanical force. In the case of electrostriction and magnetostriction there is a quadratic effect which can be made approximately linear by superposing a large constant quantity. If q is the sinusoidally changing quantity and q_o the constant superposed quantity, then the exerted force, F, in the case of the quadratic relationship may be written as:

$$F = K (q_o + q)^2 = K (q_o^2 + 2q_o q + q^2)$$

If $q_o \gg q$ the change of force will be approximately proportional to q because the quadratic term q^2 is small compared to $2q_o q$. It is thus possible with polarization to obtain a number of useful transducers from the approximate linear transformation of electrical energy into mechanical

TRANSDUCER		LINEAR		LINEARIZED BY POLARIZATION		
WITH ELECTRIC FIELD	SCHEME	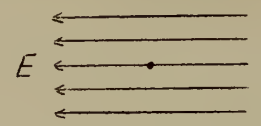			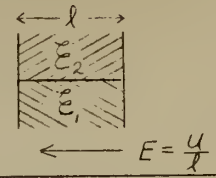	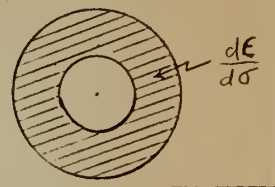
	NAME	Prototype of Transducer with Electric Field	Piezoelectric Transducer	Dielectric Transducer	Gradient E Transducer	Electrostrictive Transducer
	PRINCIPLE	Force produced by an electric field on an electric charge	Force acting on the ions of a crystal lattice	Force produced by electric charges acting upon each other	Force produced by an electric field on a Gradient E layer	Force produced by charge of dielectric constant (ϵ) with density (σ)
	FORCE EQUATION	$F = QE$	$F = \gamma U$	$F = \frac{1}{\epsilon_0 \epsilon} \frac{Q_0}{A} q$	$F = \epsilon_0 (E_2 - E_1) \frac{U_0 A}{l^2} U$	$F = \epsilon_0 \frac{d\epsilon}{d\sigma} \frac{\sigma}{(\epsilon_0 \epsilon)^2} \frac{Q_0}{A} q$
WITH MAGNETIC FIELD	SCHEME	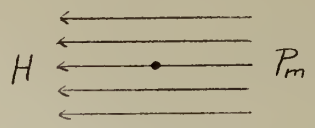	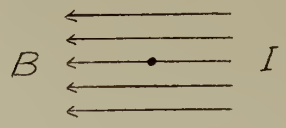		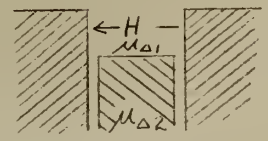	
	NAME	Prototype of Transducer with Magnetic Field	Electrodynamic Transducer	Dynamometric Transducer	Electro-magnetic Transducer	Magnetostrictive Transducer
	PRINCIPLE	Force produced by magnetic field on magnetic charge	Force produced by a magnetic field on current element	Force produced by electric currents upon each other	Force produced by a magnetic field on a gradient in permeability	Force produced by charge of μ_0 with density (σ)
	FORCE EQUATION	$F = P_m H$	$F = BIl$	$F = \frac{dL}{dx} I_0 i$	$F = \mu_0 (\mu_{a2} - \mu_{a1}) \left(\frac{N}{l}\right)^2 I_0 A i$	$F = \mu_0 \frac{d\mu_a}{d\sigma} \frac{\sigma}{(\mu_0 \mu_a)^2} \frac{\phi_0}{A} \frac{\int i dt}{N}$

Figure 1 Synoptical Table of Electromechanical Transducers

energy. Figure 1 gives a synoptical table which comprises all electromechanical transducers.

From among all the possible forms of electromechanical transducers only three have come into general use for the generation of ultrasonic waves in water; these are the magnetostrictive, the piezoelectric, and the recent electrostrictive type.

2. The Magnetostrictive Transducer

When a bar or a stack of laminated ferromagnetic material is placed with its length parallel to a large polarizing and sinusoidally changing magnetic field, the bar will change its length due to the magnetostrictive effect. The large polarizing field is used to obtain an approximate linear relation between the alternating mechanical force and displacement. The physical displacement of the bar will be the source of compressional waves into the surrounding medium. This displacement will be a maximum when the bar resonates at its natural resonant frequency, f_o, which is given by the formula:

$$f_o = \left(\frac{Y}{\rho}\right)^{\frac{1}{2}} \cdot \frac{1}{2\ell} = \frac{c}{2\ell} \quad ,$$

where ℓ is the length of the bar, Y is Youngs Modulus of elasticity, ρ is the density of the material, and c is the velocity of sound in the material.

Magnetostrictive transducers operate best in the lower ultrasonic range because of two basic limitations. (1) As the frequency becomes high the size of the bars or stacked laminated strips become smaller and more difficult to mount mechanically. (2) The electrical losses due to eddy currents increase with frequency and thus reduce the efficiency of the transducer.

3. Piezoelectric Transducer

The electromechanical behavior of the piezoelectric transducer is based on the inverse piezoelectric effect by which certain crystals undergo a change in their physical dimensions when an electric field is applied to them. This electric field is usually applied to the faces of the crystal by means of metallic electrodes. The resulting forces and displacements are usually in the same direction as the applied electric field. Maximum displacement is obtained when the crystal unit vibrates at its natural resonant frequency.

The piezoelectric phenomenon is generally confined to crystalline substances and mostly to about half of the thirty-two possible crystal classes. For a more thorough discussion into the details of crystalline structures and the various elastic and piezoelectric constants of these materials the reader will find the information available in the published works of W. Voight, W. G. Cady, and W. P. Mason. In present day usage only about three classes of crystals are used for ultrasonic transducers, these are quartz, Rochelle Salt, and ADP (Ammonium dihydrogen phosphate).

4. Electrostrictive Transducers

When certain ceramic materials are subjected to a strong electric prepolarization field they assume properties which make them very similar to piezoelectric materials. They will undergo changes in their physical dimensions, proportional to a sinusoidally varying electric field, as long as this field is small compared to the prepolarization potential. The resulting force will be an approximate linear relationship between electrical energy and mechanical energy. These ceramic materials are polycrystalline in nature and are based on titanium dioxide and alkaline

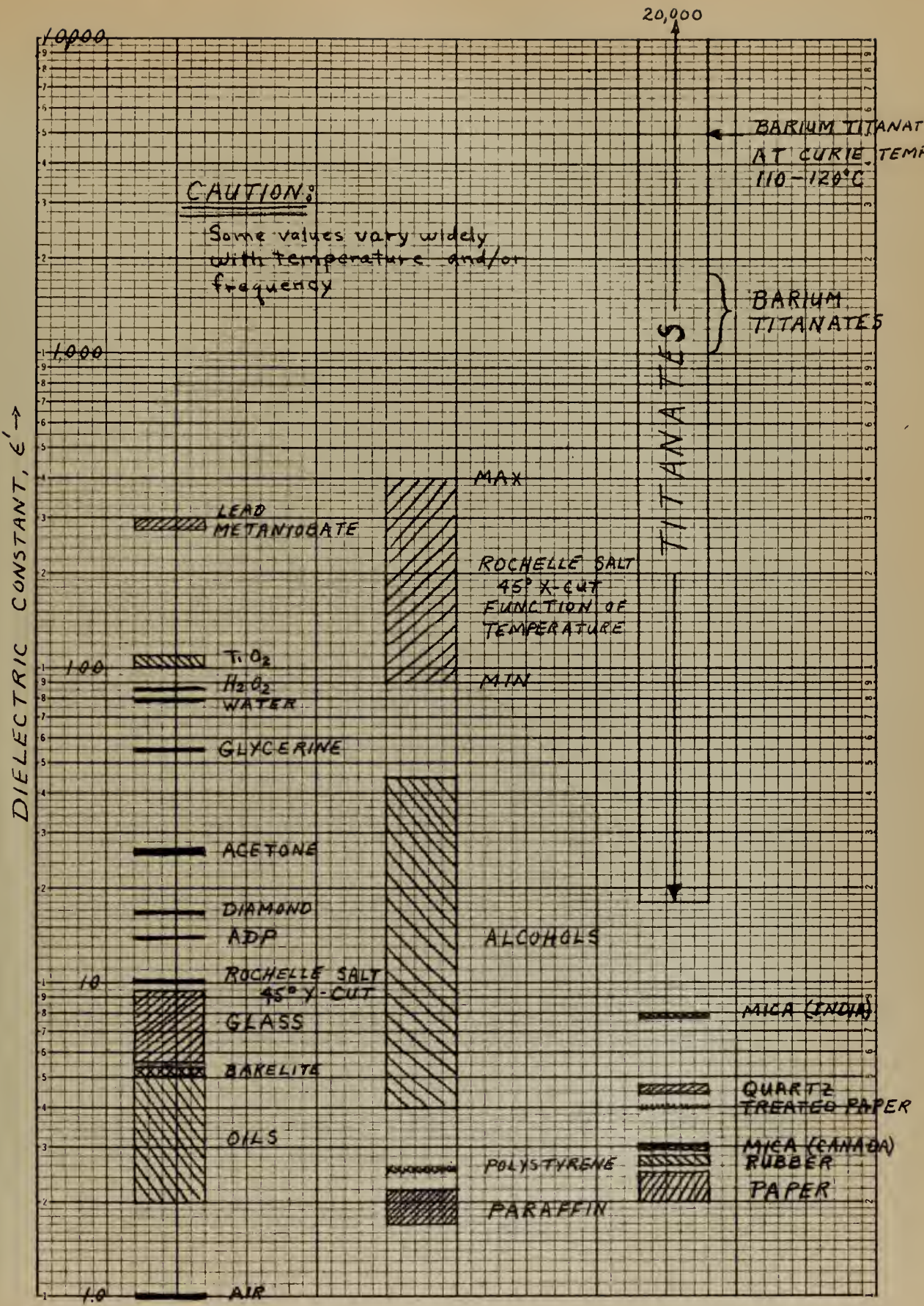

Figure 2. Table of Dielectric Constant of Various Materials

earth titanates. Their great advantage is based on the unusually high value of dielectric constant. The dielectric constant of titanates ranges all the way from thirteen for magnesium titanate up to several thousand for the solid form of barium titanate. A comparison of the various dielectric constant is given in Figure 2. The direction of the electrical and mechanical axes of these ceramics depend upon the direction of the polarizing field and thus provide an outstanding advantage for the ceramic over single crystals. The majority of the present day ceramic transducers are made of barium titanate.

5. The Advantages and Disadvantages of the Magnetostrictive, Piezoelectric and Electrostrictive Transducers.

A summary of the advantages and disadvantages of the magnetostrictive, piezoelectric and electrostrictive transducers is given in Table 1.

Table 1. The Advantages and Disadvantages of the

Magnetostrictive, Piezoelectric and Electrostrictive Transducers

TYPE	MAGNETOSTRICTIVE	PIEZOELECTRIC	ELECTROSTRICTIVE
Material	Nickel	ADP	Barium Titanate
Shock Strength	Excellent	Poor	Good
Soluability in water and solvents	Non-soluable	Poor in water	Non-soluable
Availability of material	Critical Limited Suppliers	Non-critical, but only one or two suppliers	Many suppliers
Relative cost	Medium	High	Low
Possible Efficiency	20-45%	40-50%	50-80%
Impedance level	Low	High	Moderately low
Electromechanical coupling	30%	30%	40%

CHAPTER II

BARIUM TITANATE

1. Introduction

In 1912 P. Debye suggested the existence of permanent electric dipoles, thus proposing the existence of ferroelectric materials. Since that time it has been demonstrated that these dipoles can be forced to align themselves in parallel arrays in certain solid materials and thus form a ferroelectric material with extremely high dielectric constants.

About 1940 E. Wainer and co-workers at the Titanium Alloy Manufacturing Company found that certain titanates, barium titanate in particular, had a dielectric constant of several thousand. This was about ten times higher than any of the ceramic capacitor material which had been used previously. However, this pertinent information remained restricted in this country until the end of World War II. After much of the pioneering development on this material had been partially completed, it was suggested for the construction of ultrasonic transducers. Since that time barium titanate has taken its place along with magnetostrictive metals and piezoelectric crystals in the ultrasonic transducer field.

2. Domain Structure of Barium Titanate

Barium titanate crystallizes into the simple perovskite structure which has a center of symmetry and is not piezoelectric above its Curie point of about 120°C. Figure 3 shows the ideal perovskite structure of barium titanate and it is seen that the titanium atom is at the center of the cube with the barium atoms at the corners of the cube and the oxygen atoms at the center of the faces of the cube. Thus, the structure may be employed

as a single crystal or formed into a rugged ceramic of any desirable shape.

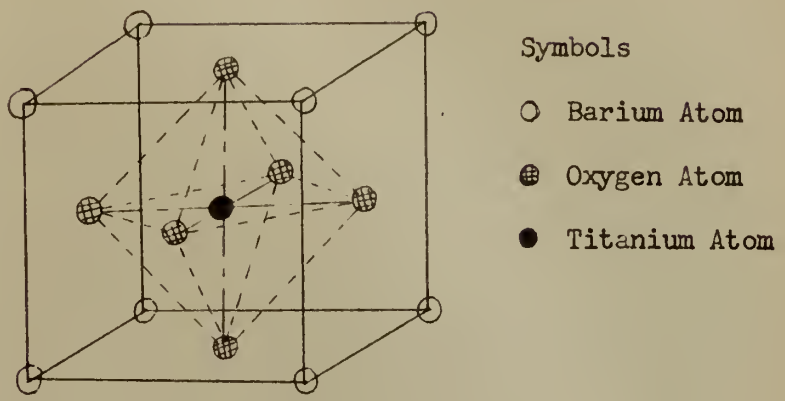

Figure 3

Perovskite Structure of Barium Titanate

As the cubic crystal is cooled below the Curie point there are a series of three phase transitions, the first of these occurs just below the Curie point, about 118°C, where the crystal changes into a tetragonal shape. The polar axis is in the 100 direction and the crystal expands slightly in this direction where as in the two axis at right angles to the polar axis the crystal contracts. The amount of mechanical deformation being proportional to the square of the polarization. At about 10°C there is a second phase transition and the crystal assumes an orthorhomic configuration and the polar axis is along the 101 direction. Finally at about -70°C, the third phase transition occurs and the crystal assumes a trigonal configuration with the polar axis in the 111 direction. These phase transitions are shown in Figure 4.

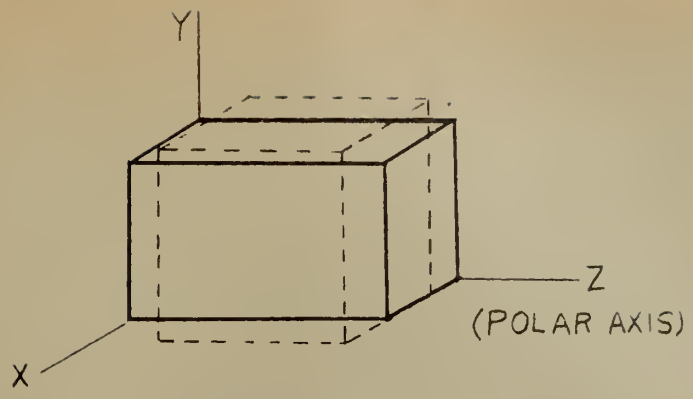

TETRAGONAL

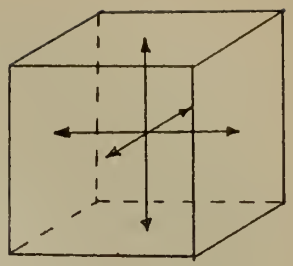

THE SIX EQUIVALENT DIRECTIONS OF THE POLAR AXIS

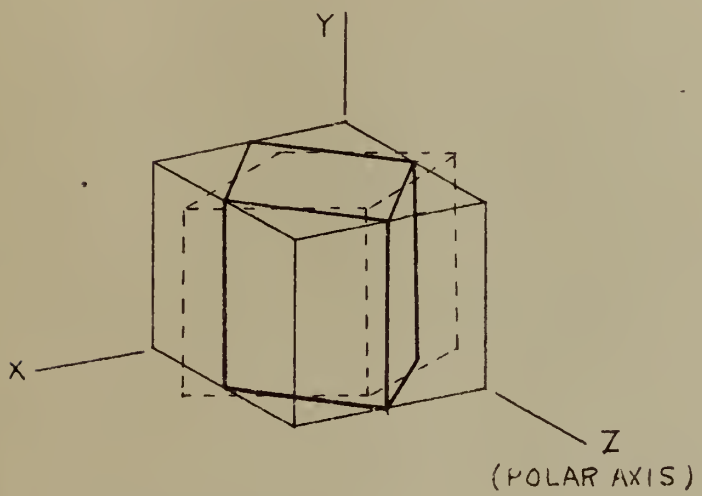

ORTHORHOMBIC

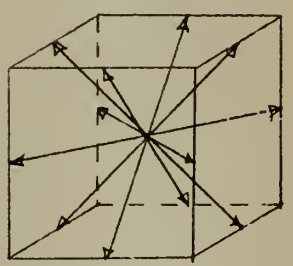

THE TWELVE EQUIVALENT DIRECTIONS

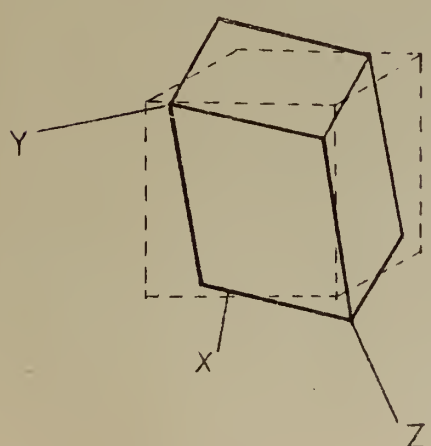

TRIGONAL

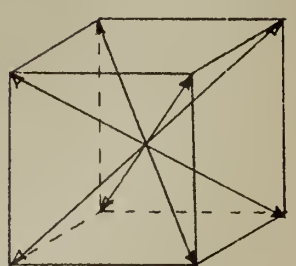

THE EIGHT EQUIVALENT DIRECTIONS

Figure 4. Ferroelectric Phases of $BaTiO_3$ and Equivalent Directions of Polar Axis

3. The Electromechanical Behavior of Barium Titanate

The relationship between strain, S_h, stress, T_h, electric field, E_h, and electric polarization, P_h, for non-ferroelectric, piezoelectric crystals is given by the following equations:

$$S_h(E,T)=\sum_{i=1}^{3} d_{ih}E_i + \sum_{i=1}^{3} g_{ih}E_i^2 - \sum_{i=1}^{6} s_{ih} T_i + \cdots \quad h=1,2,---,6 \qquad (1)$$

$$P_h(E,T)=\sum_{i=1}^{3} \chi_{ih}E_i - \sum_{i=1}^{6} d_{ih}T_i \qquad h=1,2,3 \qquad (2)$$

where χ_{ih} are the components of the electric susceptibility, s_{ih} the elastic compliance coefficients, while d_{ih} and g_{ih} are the first and second order piezoelectric coefficients, respectively. The first term of equation (1) represents the linear converse piezoeffect and the second term represents the second order quadratic effect which represents the electrostrictive effect. For the tetrogonal structure of barium titanate in the ferroelectric region between 10°C and the Curie temperature of about 110°C with an external field, E_z, applied along the polar axis is in the Z direction, equation (1) reduces to:

$$S_x = d_{31}E_z + g_{31}E_z^2 , \qquad (3),$$

the strain component along the X-axis, and

$$S_z = d_{33}E_z + g_{33}E_z^2 , \qquad (4)$$

the strain component along the Z-axis. These equations are also applicable above the Curie point, but the first order piezoelectric coefficients d_{ih} are zero due to the fact that the material has a center of symmetry in

the cubic range. The ferroelectric properties of barium titanate differ from other piezoelectric crystals in two ways: In the first place, there is a spontaneous polarization whose magnitude depends upon the temperature and applied external field, and thus the piezoelectric coefficients are dependent upon these parameters. Secondly, the domain structure of these crystals change with the applied field and thus cause additional changes in the strain components.

The effect of this spontaneous polarization can be explained in the following manner. If we let P_o be the spontaneous polarization which is directed along the polar axis (Z-axis) of the crystal, and $(S_x)_o$ and $(S_z)_o$ be the spontaneous strain components in the X- and Z- directions, respectively, taken relative to the dimensions of the crystal at the Curie point, it has been demonstrated that the following relations are valid:

$$(S_x)_o = K_1 P_o^2 \tag{5}$$

$$(S_z)_o = K_2 P_o^2 \tag{6}$$

where K_1 and K_2 are constants. In these equations $(S_x)_o$ corresponds to a contraction and $(S_z)_o$ to an elongation.

When an external field is applied along the polar axis, there is an additional "external" polarization P_z, and there is an incremental change in the respective strain components and equations (5) and (6) become

$$S_x = (S_x)_o + \Delta S_x = K_1 (P_o + P_z)^2 \tag{7}$$

$$S_z = (S_z)_o + \Delta S_z = K_2 (P_o + P_z)^2 \tag{8}$$

Expanding these equations and substituting from equations (5) and (6) we obtain,

$$\Delta S_x = (2K_1P_o)P_z + K_1P_z^2 \tag{9}$$

$$\Delta S_z = (2K_2P_o)P_z + K_2P_z^2 \tag{10}$$

From equation (2) we can write $P_z = \chi_c E_z$, where χ_c is the susceptibility in the Z-direction and thus the incremental changes in strain become,

$$\Delta S_x = (2K_1\chi_c P_o)E_z + (K_1\chi_c^2)E_z^2 \tag{11}$$

$$\Delta S_z = (2K_2\chi_c P_o)E_z + (K_2\chi_c^2)E_z^2 \tag{12}$$

Comparing these equations with equations (3) and (4) we see that:

$$\begin{aligned} d_{31} &= 2K_1\chi_c P_o, & d_{33} &= 2K_2\chi_c P_o \\ g_{31} &= K_1\chi_c^2 & g_{33} &= K_2\chi_c^2 \end{aligned} \tag{13}$$

Thus, by knowing the initial electric susceptibility, the piezoelectric coefficients of barium titanate can be calculated for any temperature and the incremental changes in strain calculated for any applied external field. However, this is only valid in the case where the internal field is very much smaller than the linear effect and may be neglected. Figure 5 shows an example of the region in which the above linear piezoelectric relations are valid.

4. The Effects of Additives to Barium Titanate

The physical properties of barium titanate may be altered by the addition of various other titanates. Lead titanate and calcium titanate are

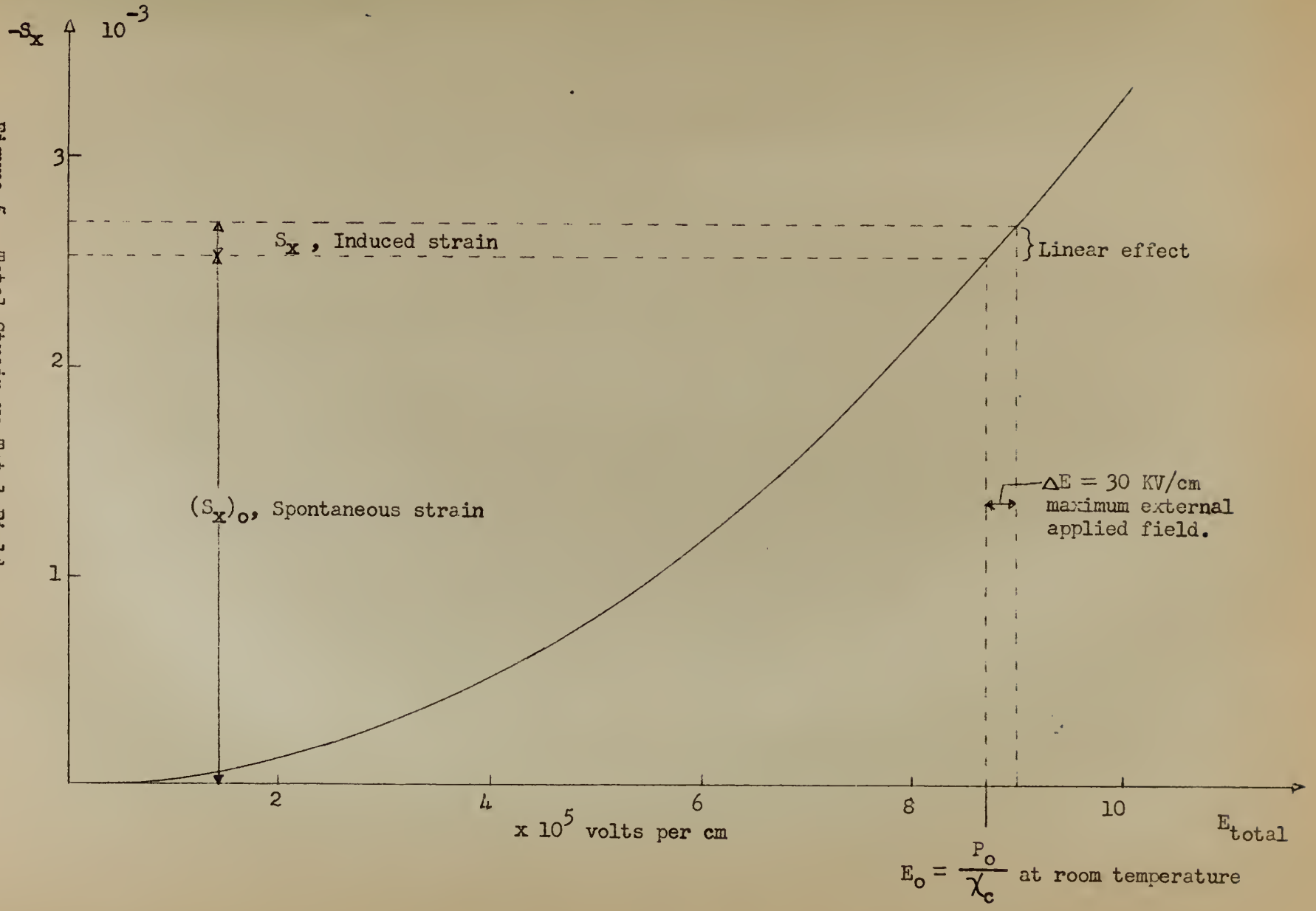

Figure 5. Total Strain vs Total Field

useful in stabilizing the piezoelectric response of barium titanate near the second transition point, about 5°C, where the orthorhombic-tetragonal inversion occurs. Figure 6 shows the depression of this transition temperature versus to percentage addition of these titanates.

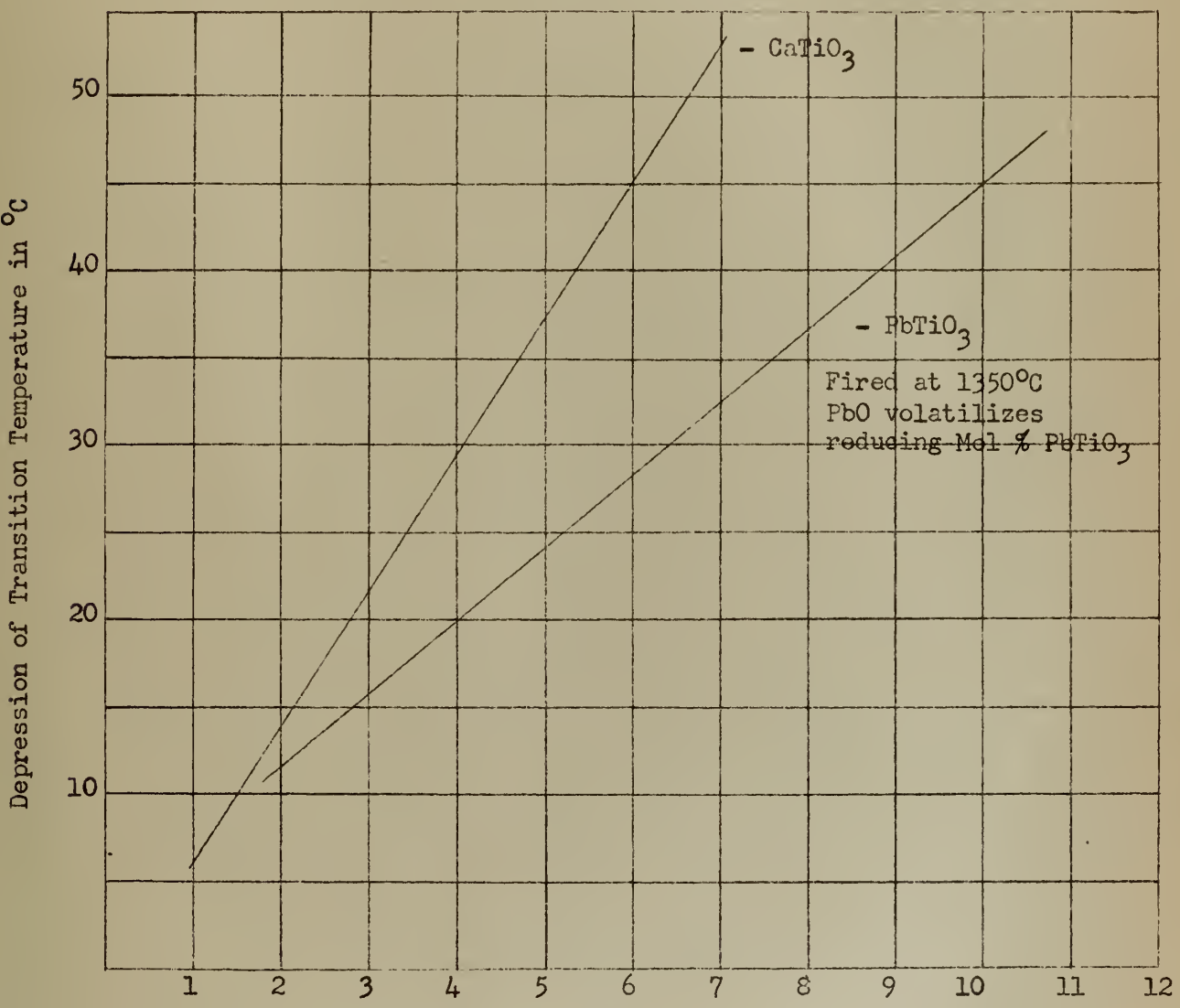

Figure 6

Depression of Second Transition Point in $BaTiO_3$

Through $PbTiO_3$ or $CaTiO_3$ Additions

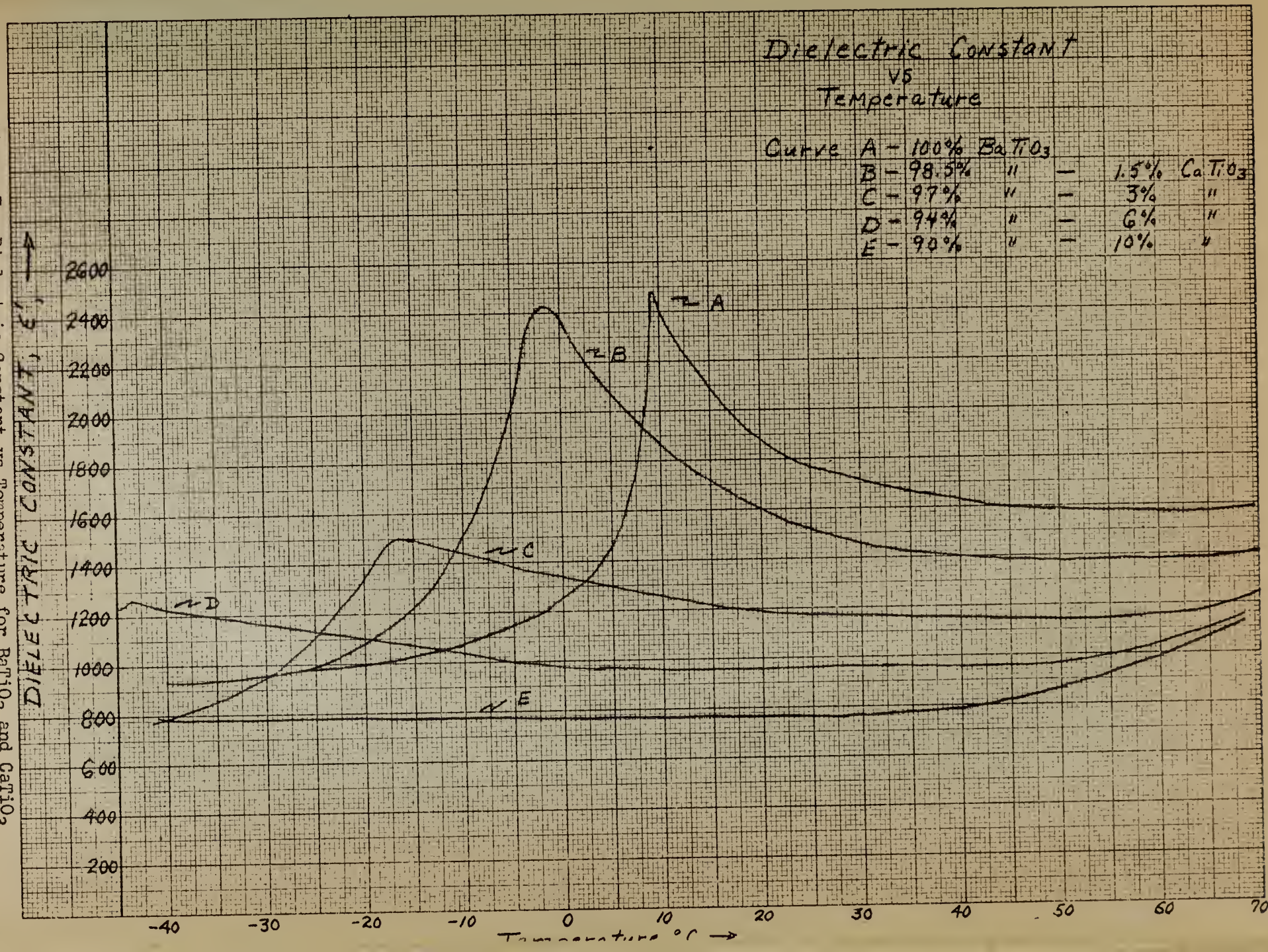

Figure 7. Dielectric Constant vs Temperature for $BaTiO_3$ and $CaTiO_3$

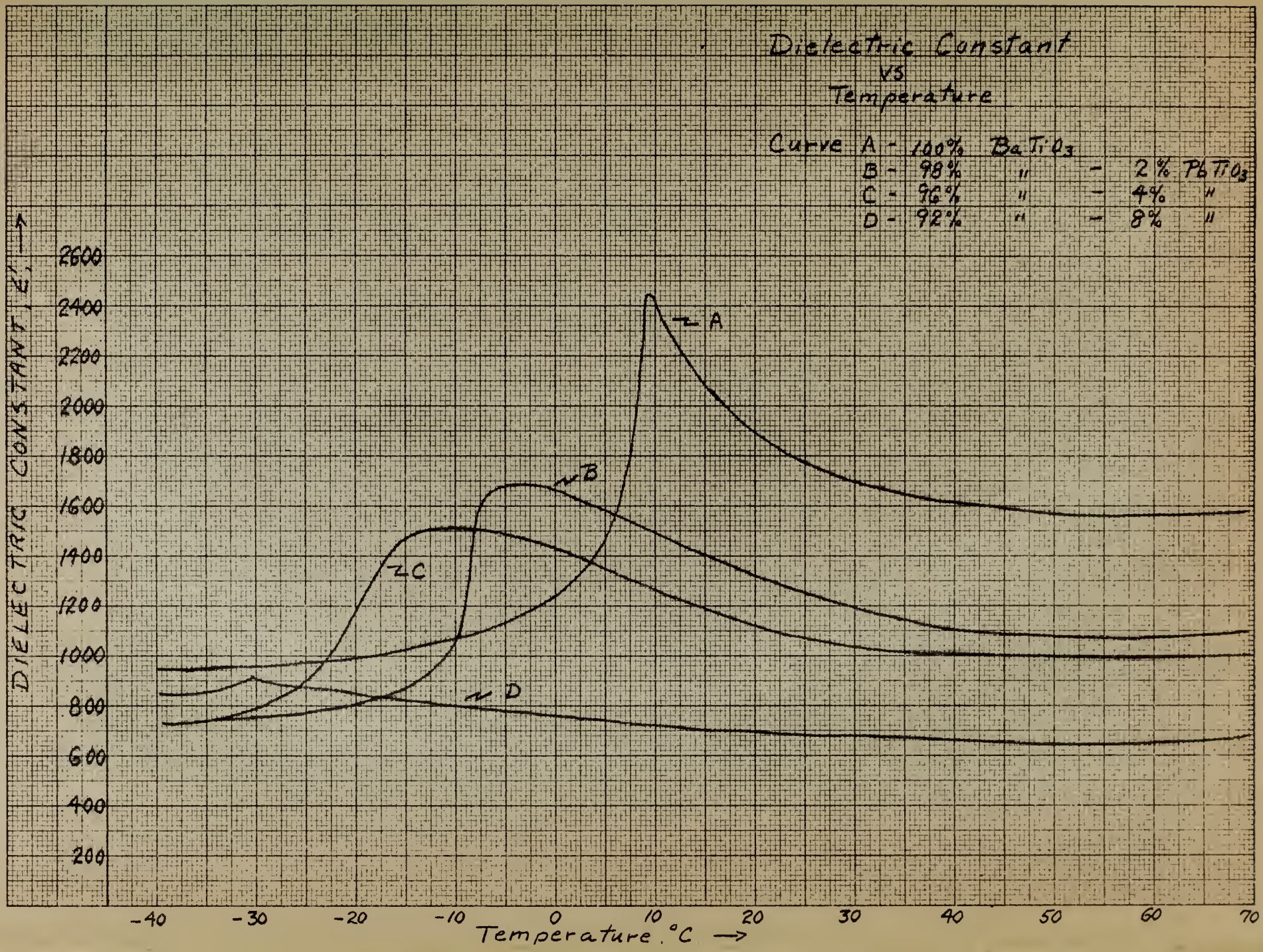

Figure 8. Dielectric Constant vs Temperature for $BaTiO_3$ and $PbTiO_3$

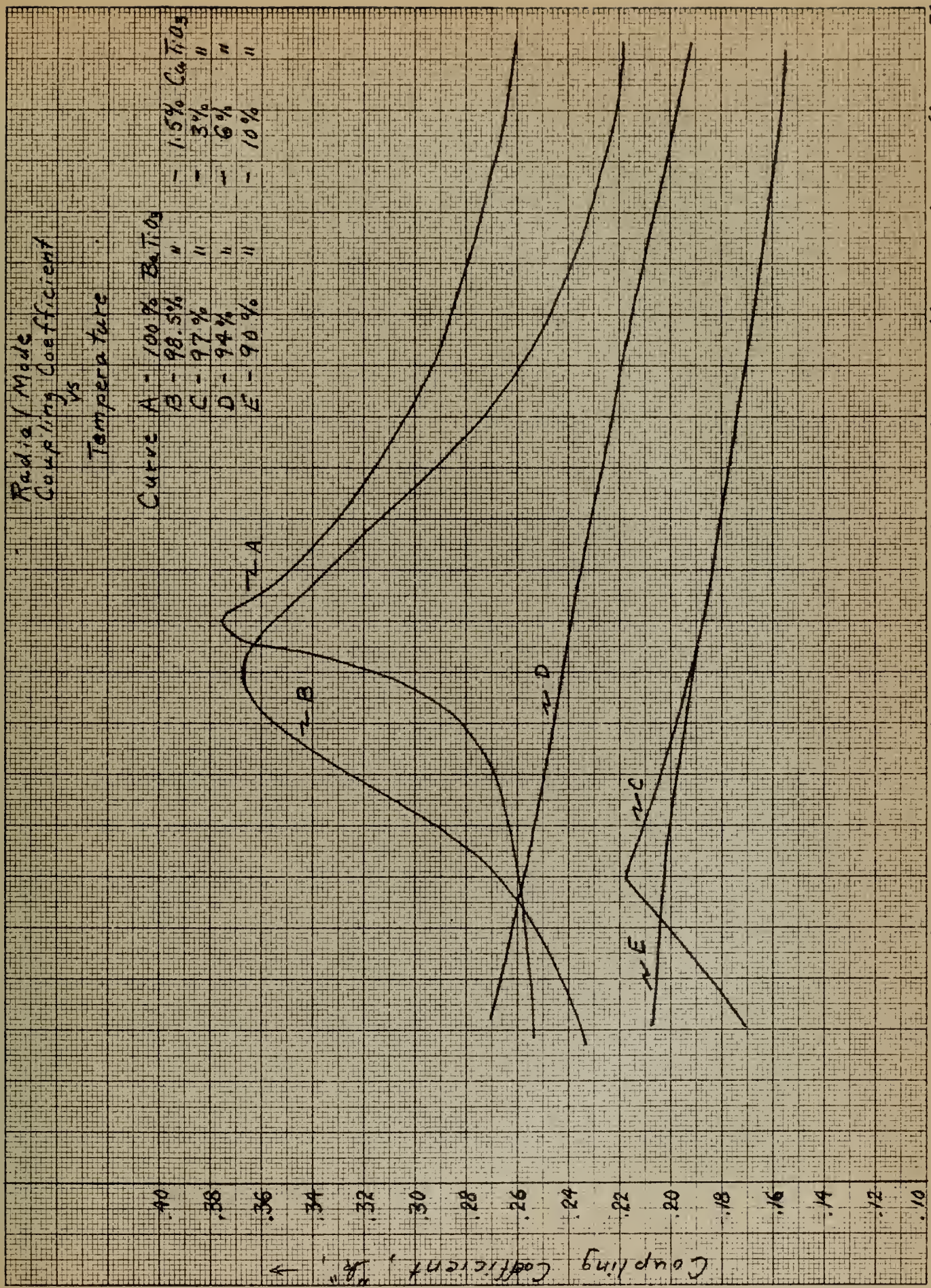

Figure 9. Radial Mode Coupling Coefficient vs Temperature for $BaTiO_3$ and $PbTiO_3$

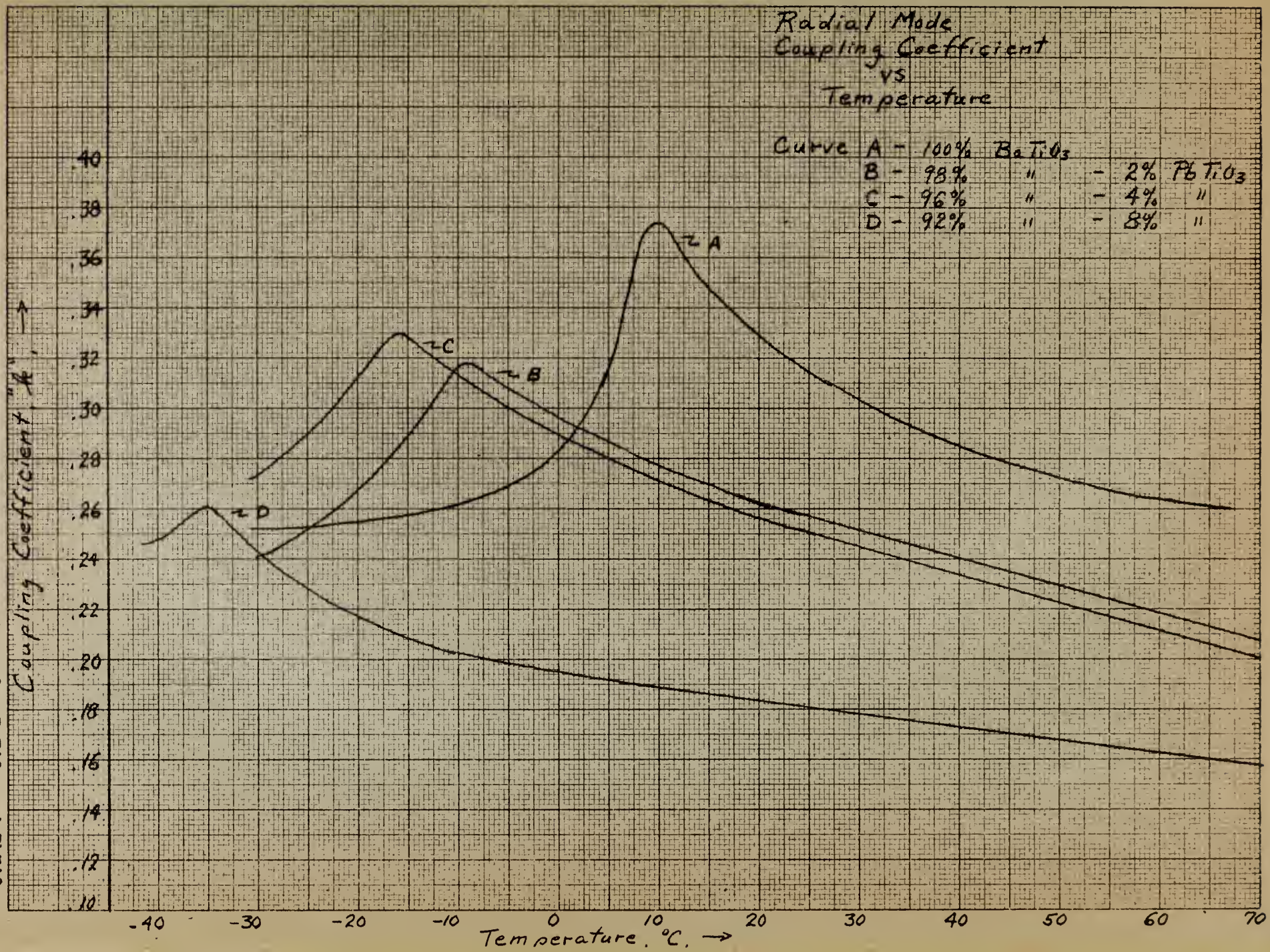

Figure 10. Radial Mode Coupling Coefficient vs Temperature for $BaTiO_3$ and $PbTiO_3$

Figures 7 to 10 show the effects on the coupling coefficient, k, and the dielectric constant, ϵ, by the addition of lead titanate and calcium titanate. It is seen from these curves that calcium titanate in the 3% to 6% range shifts the transition point down to less than -15°C while still maintaining a dielectric constant of about 1000 to 1200 over the normal operating temperature of a transducer. This is a very desirable factor to be considered in the construction of any transducer.

CHAPTER III

FABRICATION AND PROCESSING OF BARIUM TITANATE CERAMICS

1. Preparation of the Composition

The preparation of the raw material, in regards to particle size and blending of the ingredients, requires that the material be reduced to a fine powder. In some cases the raw materials must be calcined prior to being used. In general practice, the basic composition is approximately 100 per cent commercial barium titanate with certain additives used to vary the curie temperature and the value of the dielectric constant as a function of temperature. Being a non-plastic material it is essential that additional binder additives be employed to impart essential working properties to the material during the forming process. The requirements of these binders are as follows:

(A) In pressing, the additive must serve as a lubricant to facilitate the flow of the material into the mold and it should provide dry strength to permit handling prior to firing the ceramic.

(B) In extrusion, the additive must provide plasticity to allow the material to be deformed and to retain the die shape after extrusion. Dry strength is again important to provide ease of handling.

(C) In casting, the additive must form a stable suspension by preventing settling of particles. Again dry strength is required.

(D) In addition to providing the above forming and dry state properties, the binder should have no influence on the properties of the fired ceramic. This means that the binder additives should be of an organic nature which will volatilize or burn off completely with

negligible residue during firing. Polyvinyl alcohol, a product of DuPont and sold as Elvanol, has proved to be suitable as a lubricant and binder as it leaves a residue of about 0.06 per cent after fifteen minutes in air at 1200°C. Methyl cellulose, a product of the Dow Chemical Co., has also proved very satisfactory. The high solubility of the methyl cellulose insures good dispersion during drying and enables the raw material to be recovered by crushing the defective bodies and regrinding them to the desired grain size and mixed with water without further addition of binder or lubricant. Because of the high purity of methyl cellulose, the binder is completely burnt out and no organic residue remains.

2. Preparation of Ceramic Elements

There are several techniques available for the forming of the ceramic elements. The most commonly used ones being pressure molding, extrusion, slip casting, and centrifugal casting. The pressure molding method is generally used in the production of flat plate discs, rectangular blocks, or thin flat plates. Extrusion is used to form cylinders, round bar material, and in some instances thin flat plates. In the slip casting method many various forms of elements can be produced, however, this method is generally employed to produce cylindrical elements. Centrifugal casting is limited entirely to the production of cylindrical elements.

3. Firing the Ceramic Elements

After being formed and air dried, the elements are fired at about 1350-1450°C, during which treatment sintering, crystal growth, and a 15-20 per cent linear shrinkage occurs. The material must be fired for a sufficient time and temperature to insure complete vitrification. The temperature for complete vitrification is that temperature where the

porosity is a minimum and the shrinkage is a maximum. During this firing operation there are a few difficulties to be avoided. These are:

(1) Chemical reduction of the barium titanate

(2) Rupture of the element due to rapid evolution of the organic binder

(3) Rupture due to non-uniform firing shrinkage

(4) Deformation during shrinkage

(5) Thermal shock fracture due to excessively rapid heating or cooling of the material.

Globar furnance firing with the furnance loads small enough to permit free air circulation has proved to maintain a suitable state of oxidation. Gas firing requires more attention to the maintenance of an oxidizing atmosphere.

4. Grinding the Ceramic Elements

After the ceramic elements have been fired, they are then cut and machined to the required dimensions. The fired ceramic is very hard and requires either a high speed bonded abrasive or diamond wheel to perform the cutting operation. The cutting and machining operations are performed using a wet process. Ceramic disks may be cut from flat plates by the use of a brass cutting tool working in a slurry of carborundum and water. For final machining of flat plate type elements, which are required to resonate in the thickness mode, a bonded diamond wheel is generally used with a continuous flow of liquid on the wheel. This produces a fine finished surface.

5. Application of Electrodes to the Ceramic Elements

Because of the high dielectric constant and low electrical impedance of the barium titanate, it is essential that the electrodes be in intimate

contact with the ceramic and have a high conductivity. So that the electrodes will make good contact with the ceramic it is essential that the elements be cleaned in a good solvent and pre-dried prior to the application of the electrodes. The most popular electrode now in use is a conductive silver coating. This silver paste is thinned and painted on the ceramic. The dried silver is then converted to a firmly adhering silver electrode by firing the element to 700°C. It has been found that two thin layers of silver paste, with firing between successive layers, is superior to one thick layer of silver paste. The excess silver which goes "over the edge" may be removed by dressing the element on fine emery paper.

6. Activation of the Ceramic Element

Because barium titanate is polycrystalline in character and its component crystals are not oriented, there will not normally be any first order piezoelectric effect. However, when the ceramic is placed in a strong electrostatic field for an appreciable period of time, it is found that after the removal of this field the ceramic will behave as if it were piezoelectric.

There are many methods used to apply this polarizing of activation field. The most popular and generally used method is to first find the first transition or curie temperature of the ceramic; for barium titanate this is approximately 120°C. The ceramic elements are then placed in a silicon oil bath or dielectric liquid and heated to about 10°C above the curie temperature and then an electric field of ten to fifty kilovolts per inch of dielectric thickness is applied to the electrodes. The temperature is lowered slowly and the current is maintained constant by adjusting the voltage within the stated limits. The electric field is removed after the

pieces reach at least 65°C below the transition temperature. If the pieces are cooled too rapidly the ceramic may break due to unequal contraction. When the pieces have cooled sufficiently to permit handling they are again cleaned in a solvent which will remove the silicon oil or other dielectric liquid. The ceramic elements are then allowed to "age" for a period of about forty eight hours prior to evaluation of the element.

The term "aging" refers to the fact that various material parameters change as a function of time. This aging is generally logrithmic in nature and thus decreases with time. In barium titanate, after the first forty eight hours, the material parameters change very slowly. In a period of a year at room temperature the resonant frequency can vary 2% to 3%, the coupling coefficient can decrease 15%, the dielectric constant can decrease 5% to 20%, the Q_m can triple, and d_{31} decrease 5% to 25%.

CHAPTER IV

DESIGN OF A HIGHLY DIRECTIONAL HYDROPHONE

1. Introduction

The general problem was to design a highly directional hydrophone employing the principle of Modulation Scanning *. The hydrophone was to be constructed of barium titanate ceramic material with the following design specifications;

Scanning Beam	-	0.3° at - 3db
Azimuth Beam	-	6° at - 3db
Vertical Beam	-	10° at - 3db, with side lobes down at least 20db to reduce reverberation, surface and bottom reflections.
Sensitivity	-	greater than - 70 db, referred to $\frac{10 \text{ volts}}{\text{newton/m}^2}$
Operation Frequency	-	350 KCS
Efficiency	-	approximately 50%
Maximum dimensions	-	32 inches overall length

The hydrophone assembly will consist of 21 identical sections, with an overall length of the active surface of about 30 inches. This will give an azimuth beam width of approximately 0.3° at the - 3db points when all sections are in phase.

2. Section Design

In the design of the section mosaic, it was desired that the individual elements resonate at 350 KCS, in their thickness mode, when operated as a free-free bar. As barium titanate blocks will also resonate perpendicular to the direction of polarization, it was desirable that these

* The Principal of Modulation Scanning is discussed in Appendix A.

frequencies be separated at least 100 KCS from the operating frequency. Thus with an allowable section size of approximately 1.40 inches in the horizontal plane and section spacing of 1.43 inches, the size of the elements was selected as 400 x 150 x 250, (l x w x t) mils. One of the sections is shown in Figure 11, with the direction of polarization as indicated.

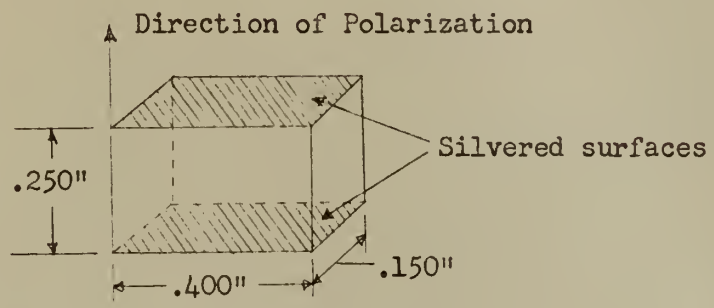

Figure 11. Size and Direction of Polarization of the Elements.

In order to achieve the desired level of the side lobes in the vertical plane a diamond shaped array was selected. Theoretically this would give side lobes down approximately 27 db and greater in contrast to the approximate 13.5 db for the pattern of a square array. In order to employ the minimum number of elements in the array the elements were arranged as shown in Figure 12.

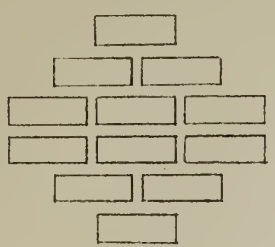

Figure 12. Layout of the Twelve Elements in the Section.

Each section will consist of 12 elements operating in their thickness mode of vibration. In order to increase the hydrophone sensitivity the elements are to be connected in a series-parallel connection as shown in Figure 13. This method of series-parallel connection will theoretically increase the hydrophone sensitivity approximately 12 db over a straight parallel connection of the 12 elements.

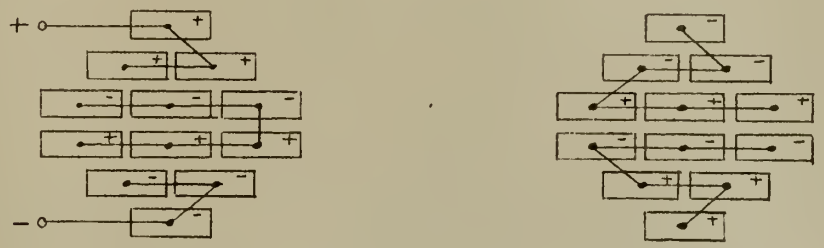

Figure 13. Series-Parallel Connection of the Section Mosaic.

In the calculation of the horizontal beam pattern, if we consider each element as a point source and then multiply this pattern by the directivity pattern of the element itself, we will obtain the predicted horizontal beam pattern. Thus we consider a point far distant from the array the horizontal beam pattern will be,

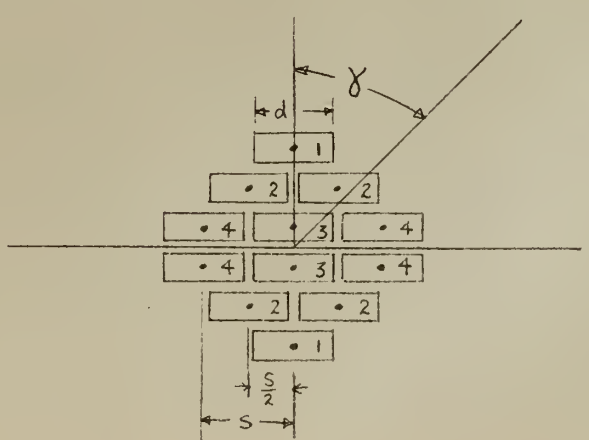

$$P_h = P_o \frac{\text{Sin } X}{X}\left[2A_1 + 2A_2\left(e^{-j\frac{1}{2}ks \text{ Sin } \gamma} + e^{j\frac{1}{2}ks \text{ Sin } \gamma}\right) + 2A_3 + 2A_4\left(e^{-jks \text{ Sin } \gamma} + e^{jks \text{ Sin } \gamma}\right)\right] \quad (1)$$

$$P_h = P_o \frac{\text{Sin } X}{X}\left[2(A_1 + A_3) + 4A_2\left(\frac{e^{-j\frac{1}{2}ks \text{ Sin } \gamma} + e^{j\frac{1}{2}ks \text{ Sin } \gamma}}{2}\right) + 4A_4\left(\frac{e^{-jks \text{ Sin } \gamma} + e^{jks \text{ Sin } \gamma}}{2}\right)\right] \quad (2)$$

$$P_h = 2P_o \frac{\text{Sin } X}{X}\left[A_1 + A_3 + 2A_2\text{Cos}(\tfrac{1}{2}ks \text{ Sin } \gamma) + 2A_4\text{Cos}(ks \text{ Sin } \gamma)\right] \quad (3)$$

Where

$$X = \frac{\pi d}{\lambda} \text{ Sin } \gamma \quad (4)$$

and $\frac{\text{Sin } X}{X}$ is the directivity of the individual element. If we use uniform illumination of $A_1 = A_2 = A_3 = A_4 = A$, and if we let

$$\tfrac{1}{2}ks \text{ Sin } \gamma = \theta \quad (5)$$

then equation (3) reduces to

$$P_h = 4P_oA \frac{\text{Sin } X}{X}\left[1 + \text{Cos } \theta + \text{Cos } 2\theta\right] \quad (6)$$

And by fundamental identities this further reduces to,

$$P_h = 4P_oA \frac{\text{Sin } X}{X}\left[2 \text{ Cos}^2\theta + \text{Cos } \theta\right] \quad (7)$$

Normalizing this equation by letting $P_o = \frac{1}{12A}$ we obtain the predicted

horizontal beam pattern,

$$P_h = \frac{\text{Sin } X}{X} \left[\frac{2 \text{ Cos}^2\theta + \text{Cos } \theta}{3} \right] \qquad (8)$$

Investigating this equation with a spacing, s equal to 0.460 inches, we see that;

			db down
1st null occurs at	$\theta = .500\pi$	$\gamma = 10.6^\circ$	∞
1st side lobe occurs at	$\theta = .580\pi$	$\gamma = 12.3^\circ$	> 30
2nd null occurs at	$\theta = .667\pi$	$\gamma = 14.2^\circ$	∞
2nd side lobe occurs at	$\theta \leq \pi$	$\gamma = 19.0^\circ$	> 22

A plot of the azimuth beam pattern is shown in Figure 22.

In like manner, the vertical beam pattern can be calculated as follows:

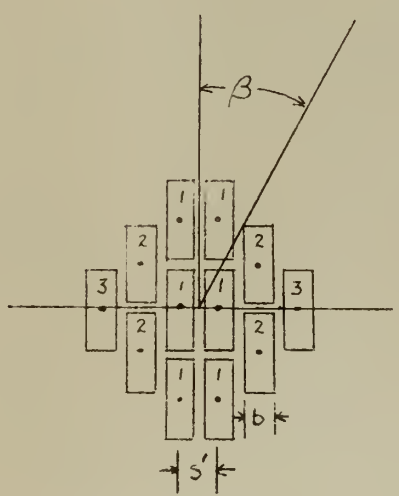

$$P_v = P_o \frac{\text{Sin } Y}{Y} \left[A_1 \left(e^{j\phi} + e^{-j\phi} \right) + A_2 \left(e^{j3\phi} + e^{-j3\phi} \right) + A_3 \left(e^{j5\phi} + e^{-j5\phi} \right) \right] \qquad (9)$$

where,

$$Y = \frac{\pi b}{\lambda} \sin \beta \tag{10}$$

$$\phi = \frac{\pi s'}{\lambda} \sin \beta \tag{11}$$

$$\begin{aligned} A_1 &= 3A \\ A_2 &= 2A \\ A_3 &= A \end{aligned} \tag{12}$$

Thus equation (9) reduces to

$$P_v = P_o \frac{\sin Y}{Y} 2A\left[3 \cos \phi + 2 \cos 3\phi + \cos 5\phi\right] \tag{13}$$

Normalizing by letting $P_o = \frac{1}{12A}$, we obtain the overall vertical beam pattern,

$$P_v = \frac{\sin Y}{Y}\left[\frac{3 \cos \phi + 2 \cos 3\phi + \cos 5\phi}{6}\right] \tag{14}$$

Investigating the vertical beam pattern with spacing, s' equal to 0.170 inches, we obtain;

			db down
1st null occurs at	$\phi = .250\pi$	$\beta = 14.5^\circ$	∞
1st side lobe occurs at	$\phi = .292\pi$	$\beta = 17.0^\circ$	> 30
2nd null occurs at	$\phi = .333\pi$	$\beta = 19.5^\circ$	∞
2nd side occurs at	$\phi = .416\pi$	$\beta = 24.6^\circ$	> 27
3rd null occurs at	$\phi = .500\pi$	$\beta = 30^\circ$	∞
3rd side lobe occurs at	$\phi = .584\pi$	$\beta = 35.6^\circ$	> 27
4th null occurs at	$\phi = .667\pi$	$\beta = 42^\circ$	∞
4th side lobe occurs at	$\phi = .710\pi$	$\beta = 45.2^\circ$	> 30
5th null occurs at	$\phi = .750\pi$	$\beta = 48.5^\circ$	∞
5th side lobe occurs at	$\phi = 1.00\pi$	$\beta = 90^\circ$	> 18

A plot of the vertical pattern is shown in Figure 23.

3. Equivalent Electromechanical Circuit

W. P. Mason, in the second edition of "Electro-Mechanical Transducers and Wave Filters", Article 6.32, starts with loss less piezoelectric equations and derives the following general circuit for a thickness vibrating piezoelectric crystals.

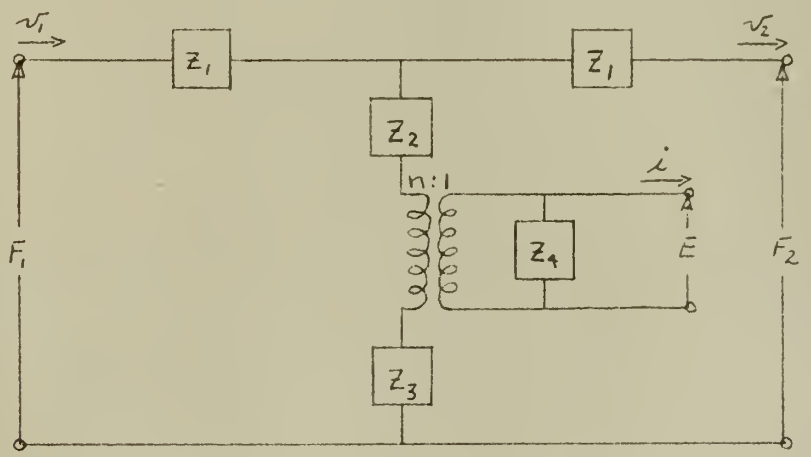

Figure 14. Equivalent Electromechanical Circuit for Thickness Vibrating Crystals.

Where,

$$Z_1 = jZ_o \text{Tan} \frac{\omega \ell}{2c}, \quad \frac{\text{Kg}}{\text{sec}} \tag{15}$$

$$Z_2 = -jZ_o \frac{1}{\text{Sin} \frac{\omega \ell}{c}}, \quad \frac{\text{Kg}}{\text{sec}} \tag{16}$$

$$Z_3 = \frac{-n^2}{j\omega C_o}, \quad \frac{\text{Kg}}{\text{sec}} \tag{17}$$

$$Z_4 = \frac{1}{j\omega C_o}, \quad \text{ohms} \tag{18}$$

$$n = k_c c \sqrt{\rho \frac{S}{\ell} C_o}, \quad \frac{\text{coulomb}}{\text{m}} \tag{19}$$

$$Z_o = \rho c S, \quad \frac{\text{Kg}}{\text{sec}} \tag{20}$$

This equivalent circuit is valid for all frequency ranges of thickness vibrating crystal operating parallel to the direction of polarization.

In the case of an air-backed transducer F_1 is equal to zero and the equivalent circuit near resonance reduces to the following form.

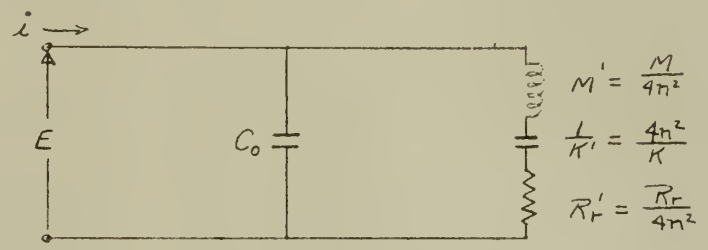

Figure 15. Equivalent Circuit for a Lossless Inertia Drive Crystal for Frequencies Near Resonance.

In the above circuit,

$$M' = \frac{l^2}{8 k_c^2 c^2 C_o} \quad , \qquad \text{henries} \qquad (21)$$

$$\frac{1}{K'} = \frac{k_c^2}{\frac{\pi^2}{8} - k_c^2} C_o \quad , \qquad \text{farads} \qquad (22)$$

$$R_r' = \frac{\rho c_1}{\rho c} \times \frac{l}{4 k_c^2 c C_o} \quad , \qquad \text{ohms} \qquad (23)$$

However, as barium titanate is not a lossless material and if we consider these losses we will obtain the following circuit,

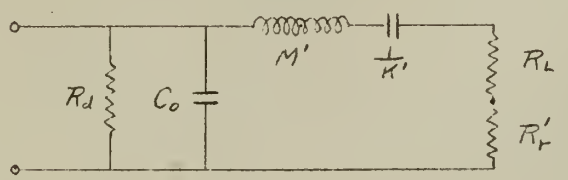

Figure 16. Equivalent Transducer Circuit for Frequencies Near Thickness Resonance

In this circuit the resistance R_d represents the dielectric losses of the material and the resistance R_L represents the losses due to internal dampening of the transducer. The value of R_L can be derived from the motional admittance diagram of the completed transducer, where

$$R_L + R_r = \frac{\omega_o M}{Q_m} \tag{24}$$

and Q_m is defined as the mechanical Q of the transducer which is determined from the motional impedance diagram. The value of R_d is equal to $\frac{1}{\omega_o C_o \tan\delta}$, where $\tan\delta$ is the dielectric loss factor which is equal to approximately 2×10^{-2} for barium titanate.

4. The Hydrophone Beam Characteristics in The Fresnel Region

The extent of the near field (Fresnel region) on the axis of a transducer is a function of the length of the array in wavelengths. The hydrophone is some one hundred and seventy-five wavelengths in length and thus the Fresnel region extends a considerable distance in range. The intensity on the axis of the array, as the range increased from zero, goes through a large number of peaks and nulls. The beam pattern in this region is not useable. The position of these peaks and nulls are given in reference 22 as,

Peak $\qquad r = \frac{D^2-(2m\lambda)^2}{8m\lambda} \qquad m = 1,2,3,\cdots$

Null $\qquad r = \frac{D^2-(2m\lambda)^2}{4m\lambda} \qquad m = 1,2,3,\cdots$

where D is the effective length of the hydrophone. The last minima occurs when $m=1$ and $r \cong \frac{D^2}{4\lambda}$. In the case of the hydrophone under consideration, this corresponds to a range of approximately one hundred and twelve feet.

The Franhaufer region, where the intensity obeys the inverse square law, does not begin until the range is somewhat greater than $\frac{D^2}{2\lambda}$; the value generally considered adequate for field measurements is about $\frac{D^2}{\lambda}$ or about four hundred and fifty feet. Figures 17 and 18 show the azimuth beam patterns for seventy-five feet and three hundred feet. It is evident that at seventy-five feet the pattern is not useable. At three hundred feet, however, the pattern is approaching that which would be expected in a far field. The pattern is slightly broader, i.e. 0.34° versus 0.29°, and the side lobes are slightly higher, i.e. -10.5 db versus -13 db. From these curves it is estimated that at ranges in excess of one hundred yards, the resolution will be substantially equal to 0.3°. At ranges less than one hundred yards, the resolution will be adversely affected and, in general, not useable with a flat face array.

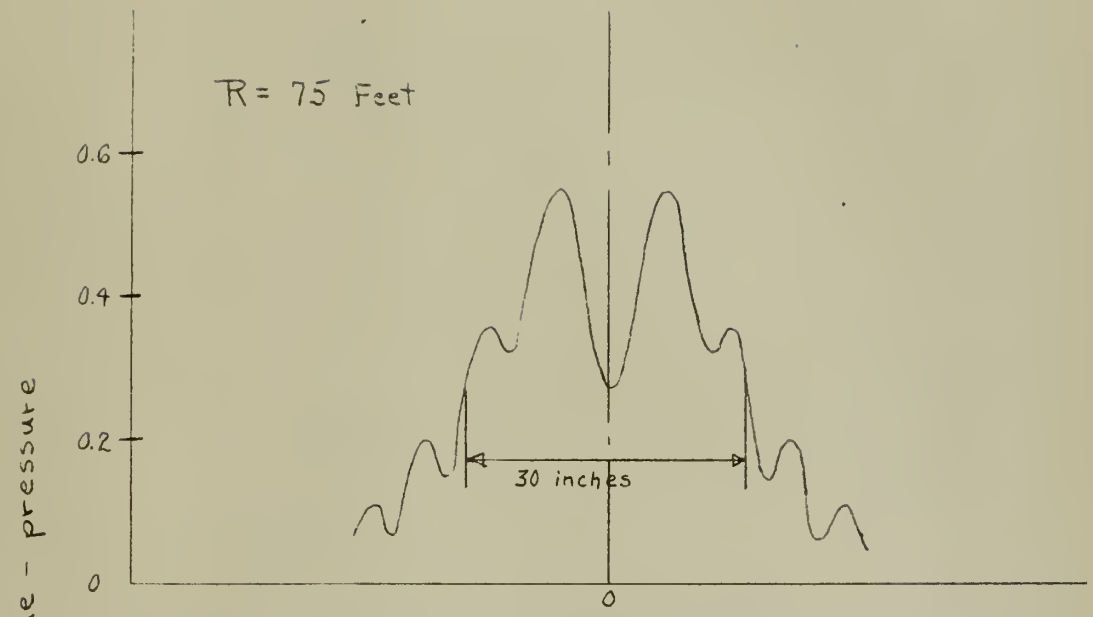

Figure 17. Hydrophone Azimuth Pattern at 75 Feet

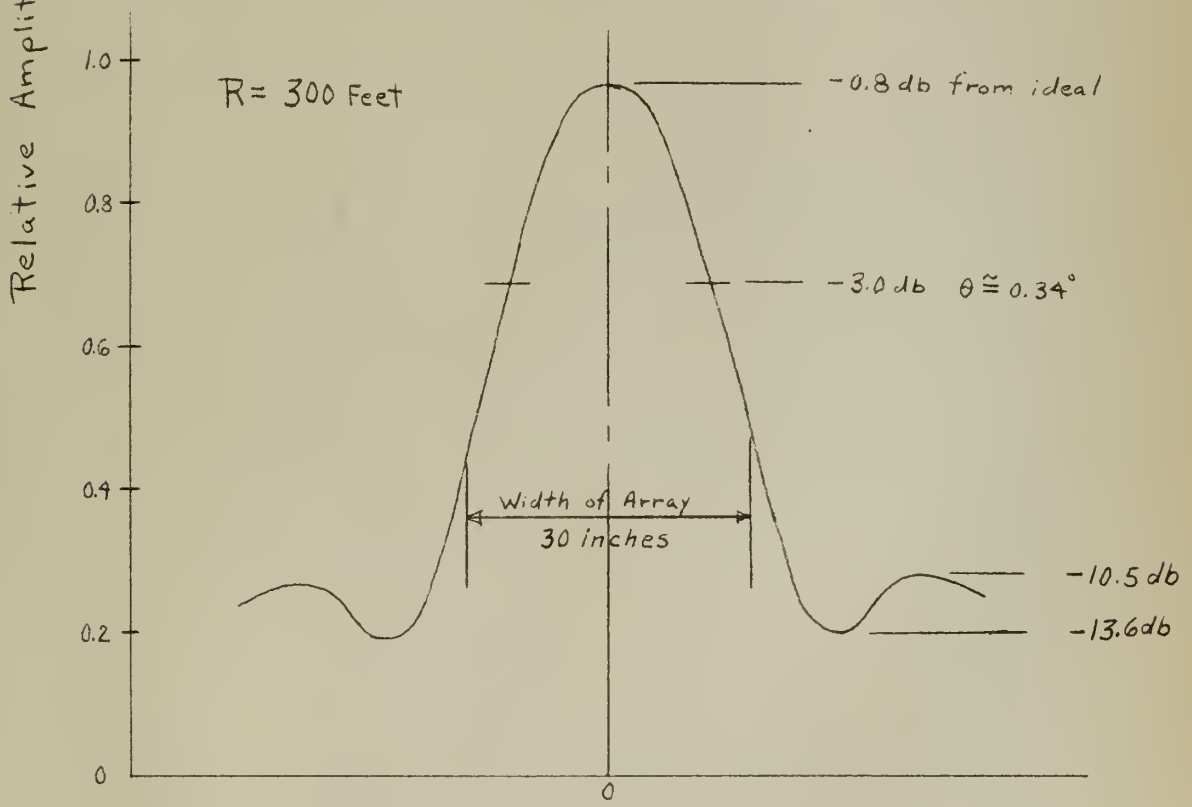

Figure 18. Hydrophone Azimuth Pattern at 300 Feet

CHAPTER V

CONSTRUCTION AND EXPERIMENTAL RESULTS OF ONE SECTION

1. Construction

The designed section mosaic was built up as shown in Figure 12. The elements were cemented together by the use of bakelite cement. The individual elements were separated by cementing coroprene between them and then the entire mosaic was encased in coroprene, with a coroprene backing. The use of coroprene backing simulates a free-free condition due to its low acoustic impedance. Also using coroprene backing enables the individual sections to be cemented to a backing plate in the transducer.

2. Impedance Measurements

The measurement of C_o was accomplished by the use of a General Radio Type 650-A Impedance Bridge and gave a C_o equal to $40\mu\mu f$. This checks closely with the calculated C_o of $39.4\mu\mu f$.

Employing the test set up shown in Figure 19, the input admittance of the section was taken in air and the resulting admittance diagram is shown in Figure 20 and the motional impedance diagram shown in Figure 21.

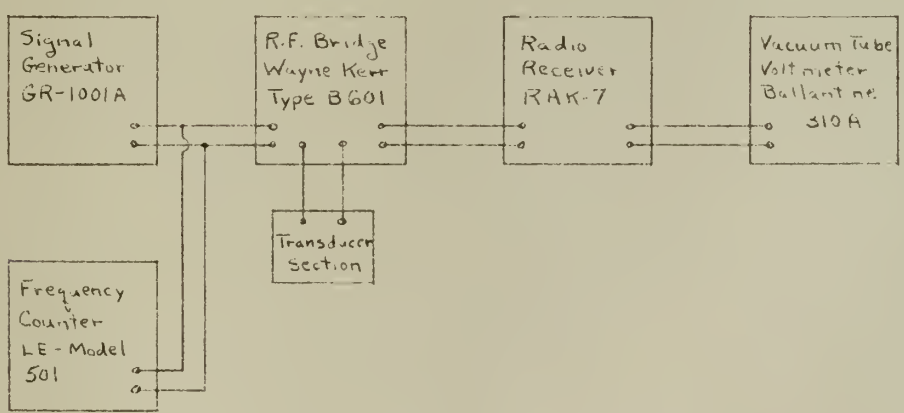

Figure 19. Test Set-up for Measuring Input Admittance

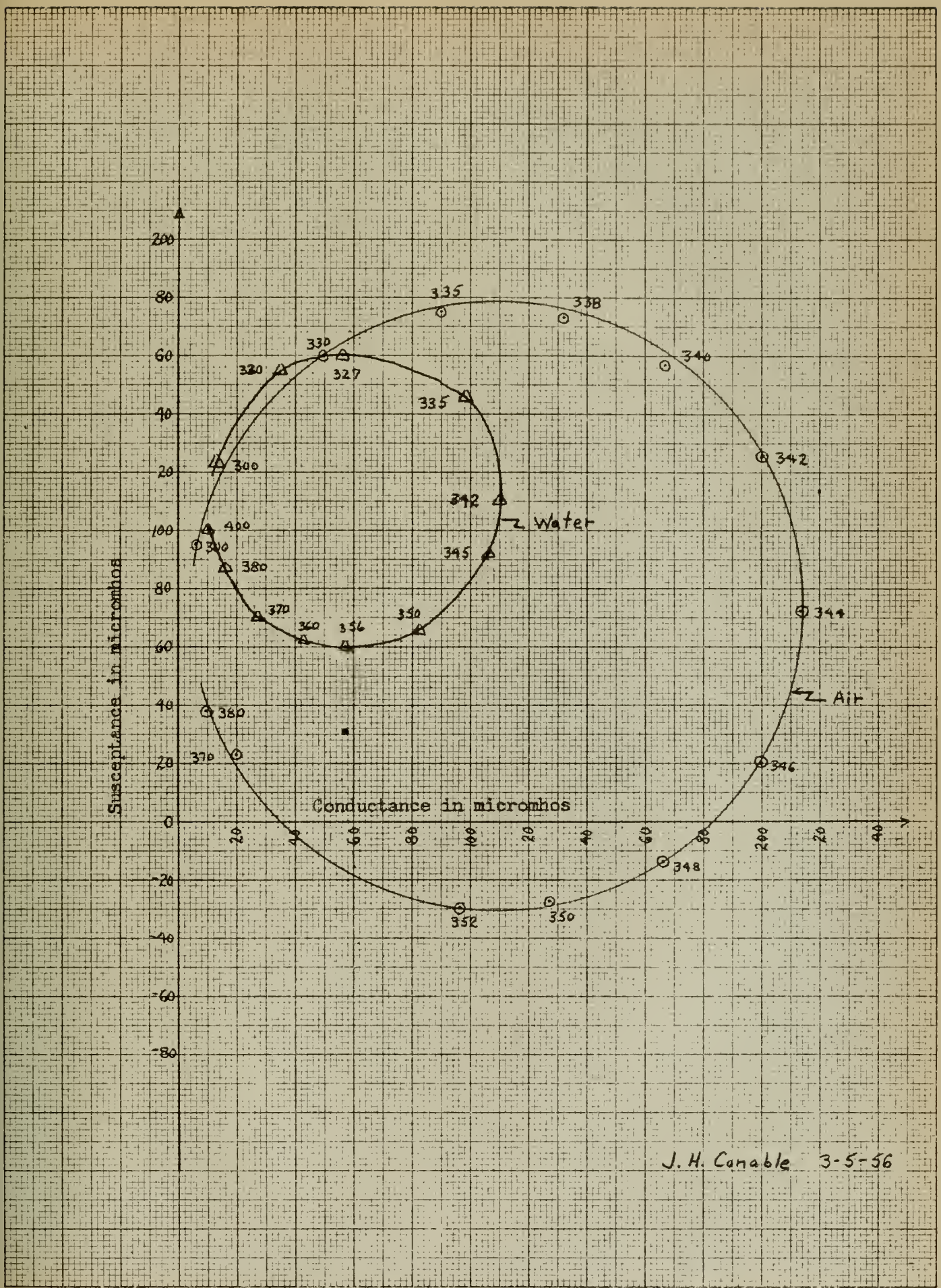

Figure 20. Input Admittance Diagram

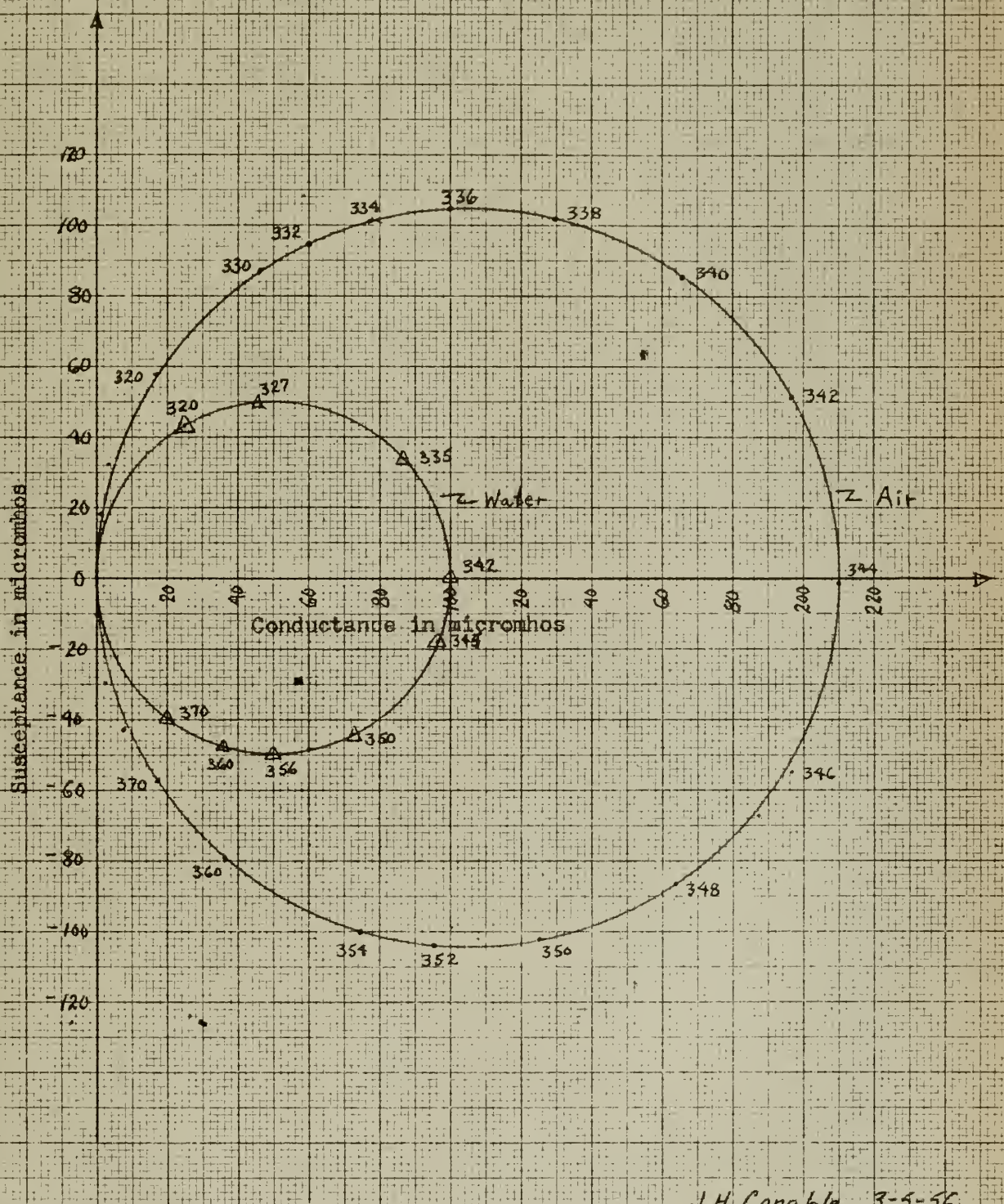

Figure 21. Motional Admittance Diagram

After the input admittance was taken in air, the mosaic was cemented to a backing plate and mounted within a test housing. The housing was filled with castor oil and a Rho-C rubber window was attached as the face plate. The assembly of the unit was done under castor oil to insure that no air was within the test transducer when the face plate was mounted. The test transducer was then placed in water and the input admittance was measured. The results are shown in Figure 20 and 21.

From the input admittance diagram the value of Q_m can be determined as;

$$Q_m = \frac{f_r}{f_2 - f_1} \tag{25}$$

where, f_r is the resonant frequency, f_1 and f_2 are the half-power point frequencies. This gives the following values.

For air Q_m equal 23.2

For water Q_m equal 11.8

The effective coupling coefficient $k_{c_{eff}}$ can also be determined as,

$$k_{c_{eff}}^2 = \frac{D_m}{B_o Q_m} \tag{26}$$

where, D_m is the diameter of the motional-admittance circle and B_o is the blocked susceptance at the resonant frequency or equal to $\omega_r C_o$. This gives the following values

For air k_c equal to 34.6%

For water k_c equal to 27.7%

3. Directivity Pattern

Using a General Radio Type 1001-A Signal Generator and a General Radio Type 1233-A Power Amplifier as the source of power the directivity patterns

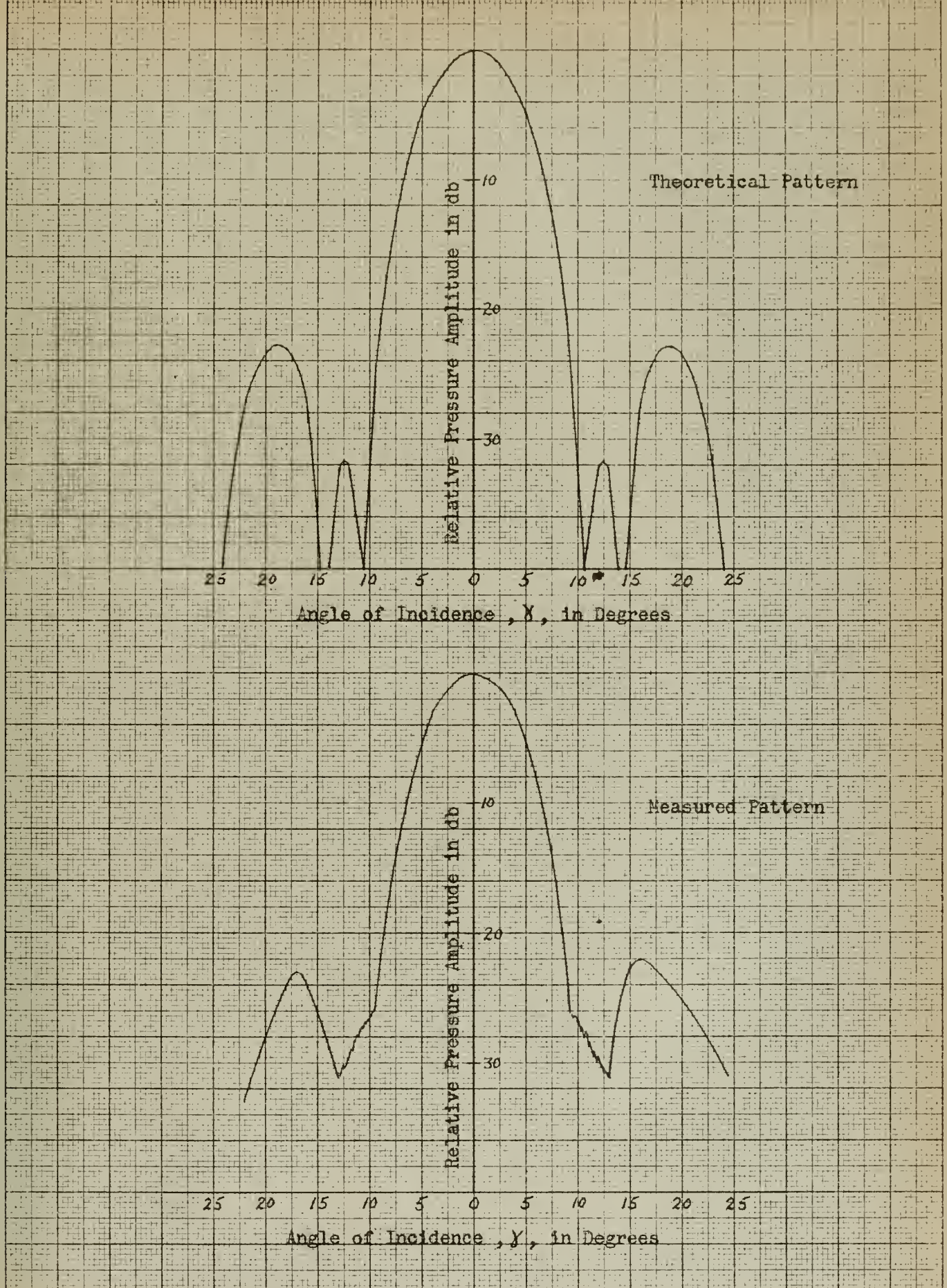

Figure 22. Section Azimuth Directivity Patterns

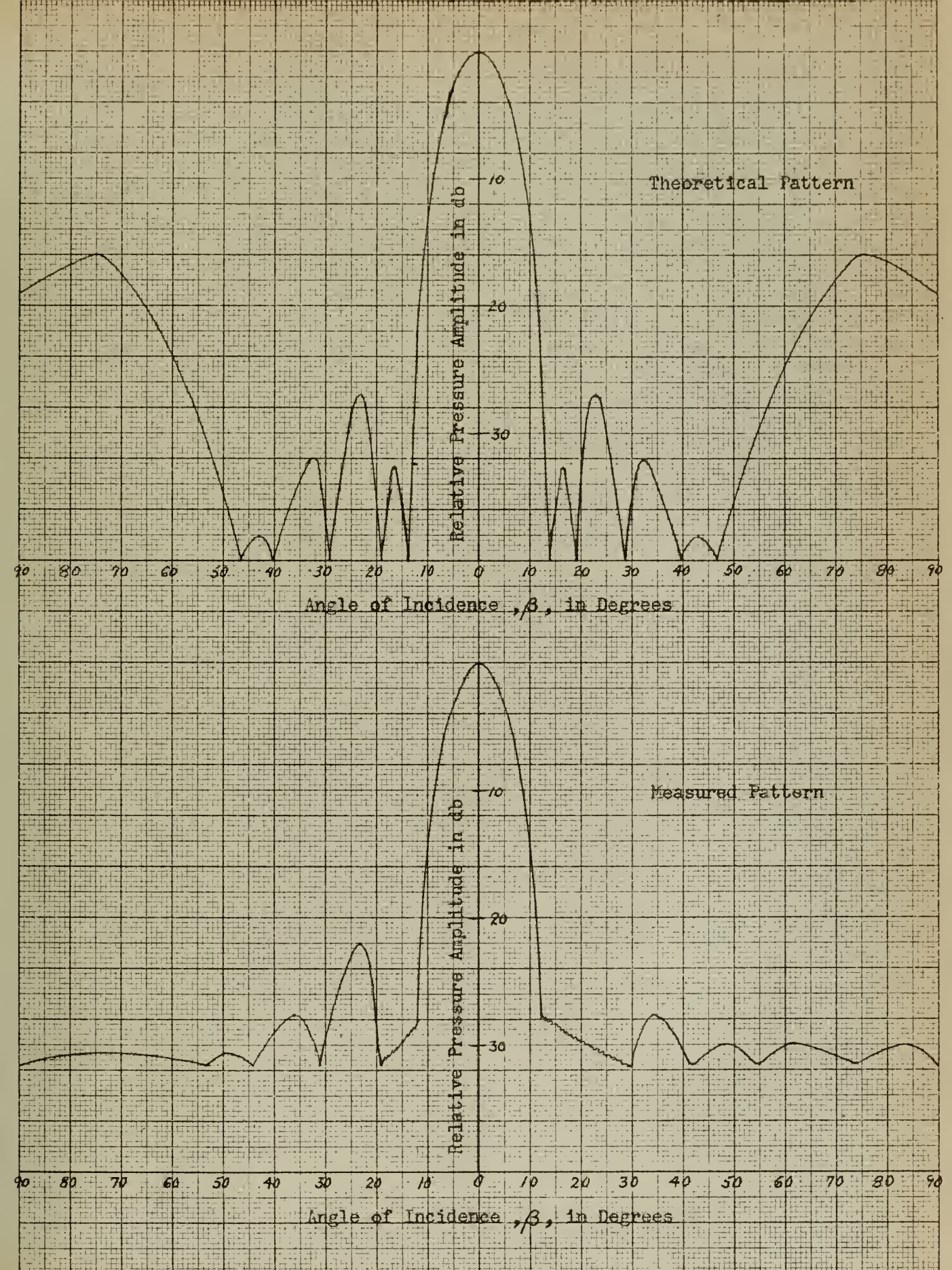

Figure 23. Section Vertical Directivity Patterns

were taken for the azimuth and vertical planes, these are shown in Figures 22 and 23. It is to be noted that the test patterns check very closely with those predicted from theory.

4. Discussion of Test Results and Conclusions.

From the admittance diagrams it is seen that the resonant frequency of the transducer is approximately 342 KCS in water. This is lower than the resonant frequency of the individual elements, which was 350 KCS. Examination of Figure 20 shows that at resonance, $\omega M' = \frac{K'}{\omega}$, or that $\ell = \frac{\lambda}{2}\left(1 - \frac{8}{\pi^2} k_c^2\right)^{\frac{1}{2}}$. Thus instead of the thickness being one-half wavelength as assumed, the thickness of the crystals should have been less than a wavelength by the factor $\left(1 - \frac{8}{\pi^2} k_c^2\right)^{\frac{1}{2}}$. The coupling coefficient can be measured by using resonance-antiresonance methods. The formula for the thickness mode of barium titanate is;

$$k_c^2 = \frac{2.52\left(\frac{f_a - f_r}{f_r}\right)}{1 + 2.52\left(\frac{f_a - f_r}{f_r}\right)}$$

A plot of $\frac{f_a - f_r}{f_r}$ versus the coupling coefficient is shown in Figure 24 and is very useful in determining the approximate value of k_c prior to assembly of an entire mosaic. This is important because the elements used for any mosaic should be selected with close coupling coefficients as well as close resonant frequency tolerances. For ceramic tubes the formula for the coupling coefficient is

$$k_c = \frac{1.417 \times 10^2 \, C_o \, (d_1 - d_2)}{\ell \quad (d_1 + d_2)}$$

where:

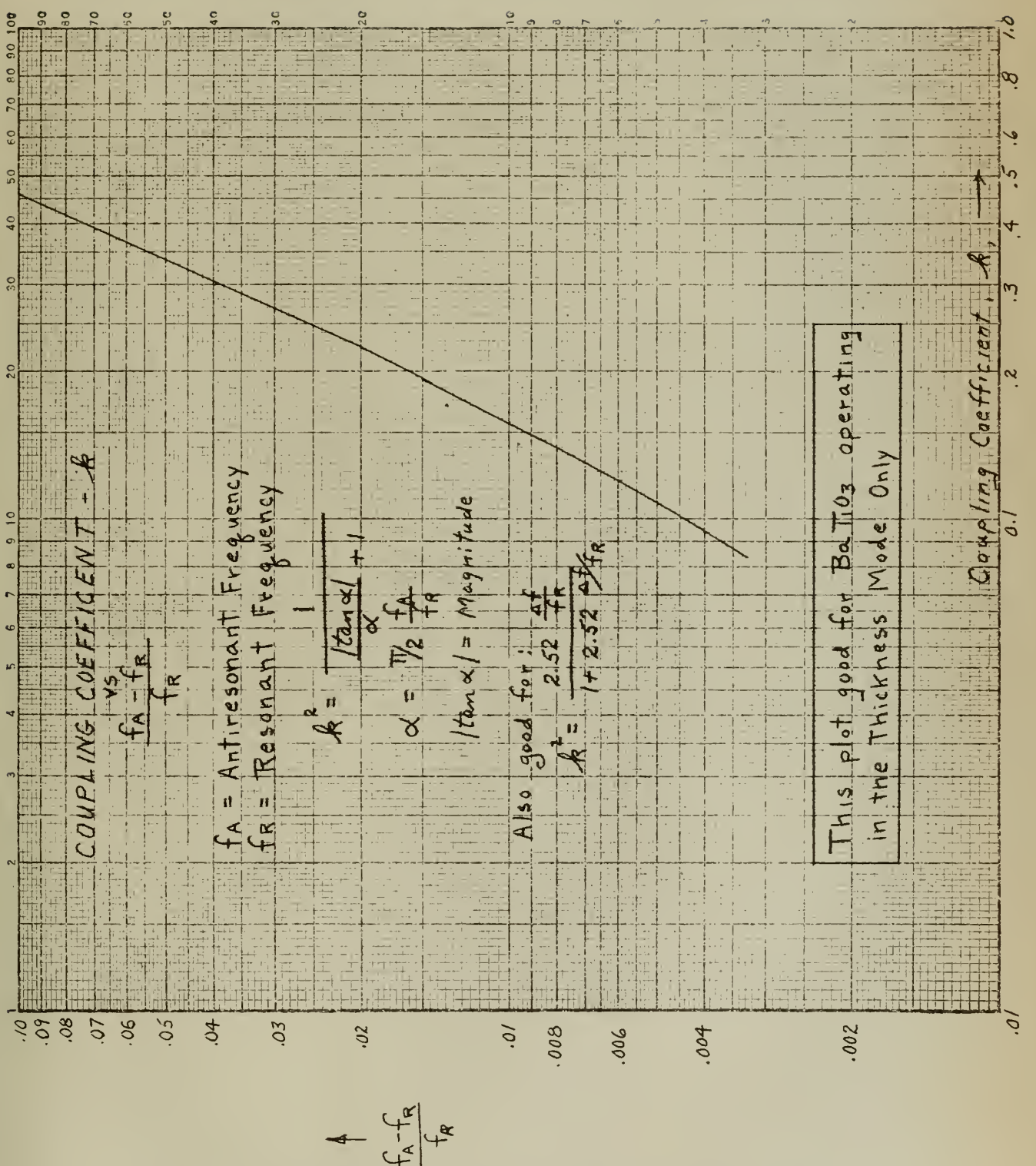

Figure 24. Coupling Coefficient for Thickness Mode $BaTiO_3$

C_o is the capacitance in farads

d_1 is the outside diameter in inches

d_2 is the inside diameter in inches

ℓ is the length of the tube in inches

Using the formula for the efficiency of a transducer derived from the motional admittance circle

$$\eta \cong \frac{D_a - D_w}{D_a}$$

where:

D_a is the diameter of the motional admittance circle in air

D_w is the diameter of the motional admittance circle in water

we obtain an efficiency of approximately 52%, which is within the limits of the design specifications. The calculated pressure sensitivity is approximately -87.8db $\frac{10 \text{ volts}}{\text{newton/m}^2}$ which also is within design specifications. Except for the fact that the resonant frequency of the section is below the specified 350 KCS the experimental results proved that the designed section is satisfactory for use in the hydrophone.

BIBLIOGRAPHY

1. Baer, J. A., "Electromechanical Devices From Ceramics", General Electric Electronics Laboratory, Report R-56-ELS-1, January 1956.

2. Baerwald, H. G. and Berlincourt, D. A., "Electromechanical Response and Dielectric Loss of Prepolarized Barium Titanate Under Maintained Electric Bias - Part I", The Journal of the Acoustical Society of America, Vol. 25, No. 4, pp 703-710, July 1953.

3. Bauer, B. B., "Piezoelectric Ceramics", Radio-Electronic Engineering, August 1948.

4. Berlincourt, D. A., "Aging of Barium Titanate Ceramics" AD-60571, Technical Report No. 4, March 30, 1955, ONR Contract No. Nonr-1055(00), Brush Laboratories Co.

5. Brochure "Piezotronic Technical Data", Brush Electronics Co.

6. Brochure, "High Dielectric Ceramics" by the Titanium Alloy Manufacturing Company, now a subsidiary of the National Lead Company.

7. Burbank, R. D. and Evans, H. T., Jr., "The Crystal Structure of Hexagonal Barium Titanate", Technical Report No. 12, Laboratory for Insulation Research, M.I.T., August 1948.

8. Camp, Leon, "Broad Band Directional Barium Titanate Transducers", The Journal of the Acoustical Society of America, Vol. 25, pp 297-301, 1953.

9. Cady, W. G., "Piezoelectricity", McGraw-Hill, New York, 1946.

10. Cady, W. G., "Progressive-Wave Method for Transducer Theory", The Journal of the Acoustical Society of America, Vol. 20, p 593, 1948.

11. Cady, W. G., "Theory of the Crystal Transducer for Plane Waves", The Journal of the Acoustical Society of America, Vol. 21, pp 65-73, 1949.

12. Caspari, M. E. and Mertz, W. J., "The Electromechanical Behavior of Barium Titanate Single Domain Crystals", Technical Report No. 30, Laboratory for Insulation Research, M.I.T., July 1950.

13. Cherry, W. L. and Adler, Robert, "Piezoelectric Effect in Polycrystalline Barium Titanate", Physical Review, pp 981-982, March 1948.

14. deBretteville, A., Jr., "Oscillographic Study of Dielectric Properties of Barium Titanate", Journal of the American Ceramic Society, Vol. 29, No. 11, pp 303-307, November 1, 1946.

15. Forsbergh, P. W., Jr., "Domain Structures and Phase Transitions in Barium Titanate", Technical Report No. 18, Laboratory for Insulation Research, M.I.T., May 1949.

16. Forsbergh, P. W., Jr., "Effect of a Two-Dimensional Pressure on the Curie Point of Barium Titanate", Technical Report No. 74, Laboratory for Insulation Research, M.I.T., October 1953.

17. Goodman, G., "Modification of the Physical Properties of Barium Titanate Ceramics", General Electric Research Laboratory Report No. RL-569, July 1951.

18. Harwood, M. G., Popper, P. and Rushman, D. F., "Curie Point of Barium Titanate", Nature, Vol. 160, pp 58-59, July 12, 1947.

19. Hueter, T. F., Neuhaus, D. P. and Kolb, J., "An Experimental Study of Polarization Effects in Barium Titanate Ceramics", The Journal of the Acoustical Society of America, Vol. 26, No. 5, pp 696-703, September 1954.

20. Hueter, T. F. and Neuhaus, D. P., "Ultrasonic Attenuation Studies in Biased Barium Titanate Ceramics", The Journal of the Acoustical Society of America, Vol. 27, No. 2, pp 292-296, March 1955.

21. Hueter, T. F. and Dozois, E., "The Frequency Response of Barium Titanate Transducers", The Journal of the Acoustical Society of America, Vol. 24, No. 1, pp 85-86, January 1952.

22. Hueter, T. F., "Sonics", John Wiley & Sons, Inc., New York, 1955.

23. Huntington, H. B. and Southwick, R. D., "Ultrasonic Velocities in Polarized Barium Titanate Ceramics", The Journal of the Acoustical Society of America, Vol. 27, No. 5, pp 947-950, September 1955.

24. Jaffe, B., Roth, R. S. and Marzullo, S., "Improvement of Piezoelectric Ceramics", AD-17282, Report No. 4, January 1 - March 31, 1953, National Bureau of Standards, NBS Project No. 0901-10-4448.

25. Jaffe, B., Roth, R. S. and Marzullo, S., "Improvement of Piezoelectric Ceramics", AD-17821, Report No. 5, April 1 to June 30, 1953, National Bureau of Standards, NBS Project No. 0901-10-4448.

26. Jaffe, B., Roth, R. S. and Marzullo, S., "Improvement of Piezoelectric Ceramics", Quarterly Progress Report No. 2, July 1 to September 30, 1952, National Bureau of Standards, NBS Project 0901-10-4448.

27. Jaffe, B., Roth, R. S. and Marzullo, S., "Improvement of Piezoelectric Ceramics", AD-26747, Report No. 6, August 17 to January 1, 1954, National Bureau of Standards, NBS Project No. 0901-10-4448.

28. Jaffe, H., "Titanate Ceramics for Electromechanical Purposes". Industrial and Engineering Chemistry, Vol. 42, pp 264-268, 1950.

29. Jaynes, E. T., "Ferroelectricity", Princeton University Press, New Jersey, 1953.

30. Kinsler, L. E., "Fundamentals of Acoustics", John Wiley & Sons, Inc., New York, 1950.

31. Koren, H. W., "Application of Activated Ceramics to Transducers", The Journal of the Acoustical Society of America, Vol. 21, pp 198-201, 1949.

32. Lane, A. L., "Design Techniques for a High Frequency Transducer with a Wide-Beam Searchlight Pattern, The Journal of the Acoustical Society of America, Vol. 25, pp 697-702, 1953.

33. Lane, A. L., "Barium Titanate Admittance-Temperature Characteristics", The Journal of the Acoustical Society of America, Vol. 25, pp 873-878, 1953.

34. Langevin, R. A., "The Electro-Acoustic Sensitivity of Cylindrical Ceramic Tubes", The Journal of the Acoustical Society of America, Vol. 26, pp 421-427, 1954.

35. Little, E. A., "The Dynamic Behavior of Domain Walls in Barium Titanate", Technical Report No. 87, Laboratory for Insulation Research, M.I.T., October 1954.

36. Madison, T. C., "Magnetostrictive Ferrite Final Report - 1954", R-55-GL-86, General Engineering Laboratory Library, Schenectady, New York.

37. Mason, W. P., "Use of Temperature and Time-Stabilized Barium Titanate Ceramcis in Transducers, Mechanical Wave Transmission Systems and Force Measurements", Proceedings of the First ICA-Congress Electro-Acoustics, W. D. Meinema, Ltd., Delft, Acustica, Vol. 4, No. 1, pp 200-202, 1954.

38. Mason, W. P., "Aging of the Properties of Barium Titanate and Related Ferroelectric Ceramics", The Journal of the Acoustical Society of America, Vol. 27, No. 1, pp 73-85, January 1955.

39. Mason, W. P. and Matthias, B. J., "Theoretical Model for Explaining the Ferroelectric Effect in Barium Titanate", Physical Review, Vol. 74, No. 11, pp 622-636, December 1948.

40. Mason, W. P., "Electrostrictive Effect in Barium Titanate Ceramics", Physical Review, Vol. 74, No. 9, pp 1134-1147, November 1948.

41. Mason, W. P., "Piezoelectric or Electrostrictive Effect in Barium Titanate Ceramics", Physical Review, Vol. 73, No. 11, pp 1398-1399, June 1948.

42. Mason, W. P., "Electrostrictive Effect in Barium Titanate", Physical Review, Vol. 72, No. 9, pp 869-870, November 1, 1947.

43. Mason, W. P., "Electromechanical Transducers and Wave Filters", 2nd Edition, D. Van Nostrand Co., Inc., New York, 1948.

44. Mason, W. P., "Piezoelectric Crystals and their Application to Ultrasonics", D. Van Nostrand Co., Inc., New York, 1950.

45. Mason, W. P. and Wick, R. F., "Barium Titanate Transducer Capable of Large Motion at an Ultrasonic Frequency", The Journal of the Acoustical Society of America, Vol. 23, p 209, 1951.

46. Matthias, B. T., "Dielectric Constant and Piezoelectric Resonance of Barium Titanate Crystals", Nature, Vol. 161, pp 325-326, February 28, 1948.

47. Matthias, B. T. and von Hippel, A., "Domain Structure and Dielectric Response of Barium Titanate Single Crystals", Technical Report No. 9, Laboratory for Insulation Research, M.I.T., February 1948.

48. Mertz, W. J., "The Electric and Optical Behavior of Barium Titanate Single-Domain Crystals, Technical Report No. 19, Laboratory for Insulation Research, M.I.T., June 1949.

49. Mertz, W. J., "The Effect of Hydrostatic Pressure on the Curie Point of Barium Titanate Crystals", Technical Report No. 29, Laboratory for Insulation Research, M.I.T., July 1950.

50. National Defense Research Committee, Div. 6, Vol. 12, "Design and Construction of Crystal Transducers".

51. National Defense Research Committee, Div. 6, Vol. 13, "Design and Construction of Magnetostrictive Transducers".

52. Pritchard, R. L., "Calculation of Acoustic Loading for an Array of Vibrating Circular Discs", General Electric Research Laboratory Report EC-1, March 1952.

53. Pritchard, R. L., "Repeated Major Lobe in Directivity Pattern from a Linear Array of Directional Acoustic Radiators", General Electric Research Laboratory Report EC-3, April 1952.

54. Pritchard, R. L., "Optimum Directivity Patterns for Linear Point Arrays", The Journal of the Acoustical Society of America, Vol. 25, pp 879-891, 1953.

55. Pritchard, R. L., "Maximum Directivity Index of a Linear Point Array", The Journal of the Acoustical Society of America, Vol. 26, pp 1034-1039, 1954.

56. Reitz, J. R. and Mueser, R. E., "Two Parabolic Underwater Transducers", The Journal of the Acoustical Society of America, Vol. 19, p 35, 1947.

57. Roberts, S., "Dielectric and Piezoelectric Properties of Barium Titanate", The Physical Review, Vol. 71, No. 12, pp 890-895, June 15, 1951.

58. Sherry, W. L., Jr. and Adler, R., "Piezoelectric Effect in Polycrystalline Barium Titanate", The Physical Review, Vol 73, No. 10, p 1230, May 15, 1948.

59. Statton, W. O., "The Phase Diagram of the Barium Titanate System, Technical Report No. 31, Laboratory for Insulation Research, M.I.T., April 1950.

60. Tucker, D. G., "An Azimuth Scanning System Using Modulation", U.D.E., Pamphlet No. 141, April 1952.

61. Von Hippel, A., Breckenridge, R. G., Chesley, F. G. and Tisza, L., "High Dielectric Constant Ceramics", Industrial and Engineering Chemistry, Vol. 38, No. 11, pp 1097-1109, November 1946.

62. Von Hippel, A., "Dielectric Materials and Applications", John Wiley & Sons Inc., 1954.

63. Von Hippel, A., "Dielectric and Waves", John Wiley & Sons Inc., 1954.

64. Wainer, E., "High Titania Dielectrics", Transactions of the Electrochemical Society, Vol. 89, pp 331-356, 1946.

APPENDIX I

THE PRINCIPLE OF MODULATION SCANNING

Figure 1 shows N transducer sections whose output signals are all identical except for phase and are represented by;

$$A \ \mathrm{Cos}\ (\omega t + \theta_r) \qquad (1)$$

where θ_r is the phase of the r^{th} section numbered outward from the center of the array and counting the center section as number zero. These signals are each modulated by a local frequency, different for each section, represented as;

$$\mathrm{Cos}\ (s + rp)t \qquad (2)$$

for the r^{th} section.

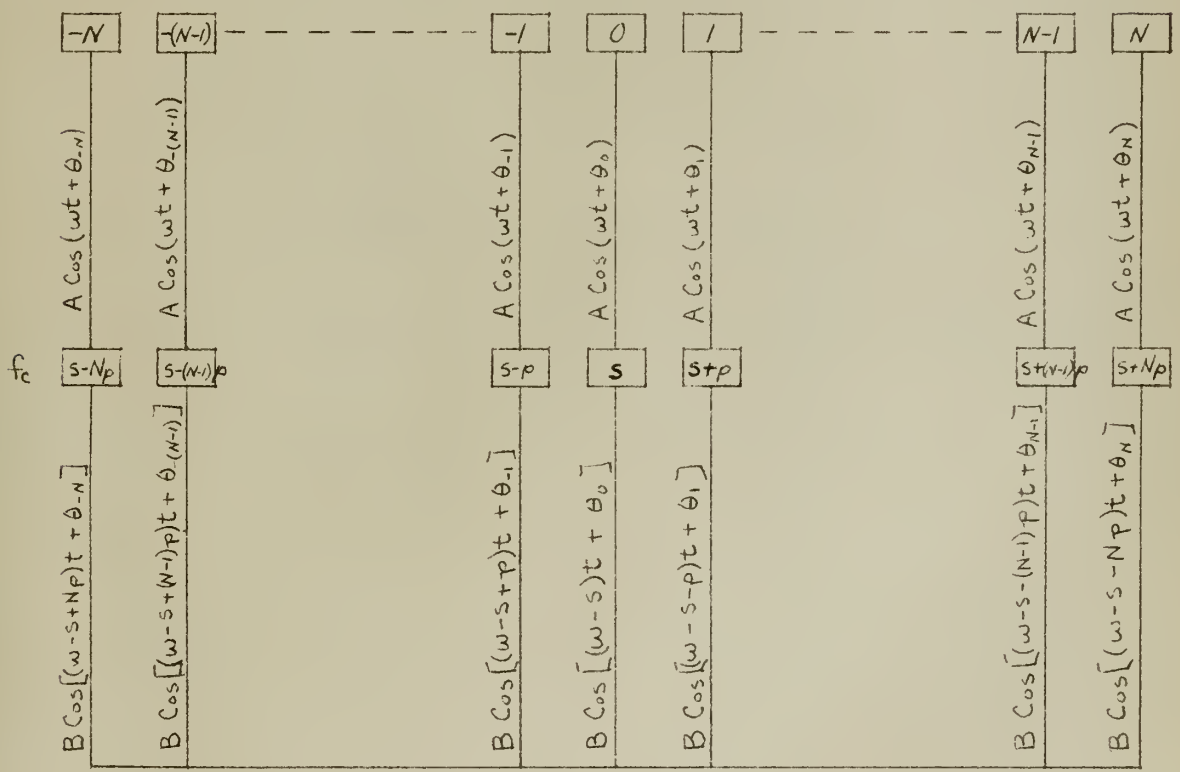

Figure 1

The output of the modulators are added together, giving a total output proportional to;

$$\sum_{r=-N}^{N} A \ \text{Cos}\ (\omega t + \theta_r)\ \text{Cos}\ (s - rp)t \tag{3}$$

Now if the signal wave received by the hydrophone is plane, and if the sections are uniformly spaced;

$$\theta_r = r\theta \tag{4}$$

where θ is proportional to the sine of the angle of incidence and is equal to;

$$\theta = \frac{2\pi d}{\lambda} \text{Sin}\ \gamma \tag{5}$$

where;

$d \doteq$ center to center spacing of the sections

$\lambda \doteq$ wavelength of the acoustic signal

$\gamma \doteq$ angle of incidence relative to the normal to the hydrophone face.

Thus the output in Figure 1 is proportional to

$$B \sum_{r=-N}^{N} \text{Cos}\left[\ (s - \omega + rp)t - r\theta\right] + B \sum_{r=-N}^{N} \text{Cos}\left[\ (s + \omega + rp)t + r\theta)\right] \tag{6}$$

$$= B\ \text{Cos}(s - \omega)t \left[1 + 2 \sum_{r=1}^{N} \text{Cos}\ r(pt - \theta)\right] + \tag{7}$$

$$B\ \text{Cos}(s + \omega)t \left[1 + 2 \sum_{r=1}^{N} \text{Cos}\ r(pt + \theta)\right]$$

The output thus consists of two carriers, $(s - \omega)$ and $(s + \omega)$, each modulated by the function

$$1 + 2 \sum_{r=1}^{N} \text{Cos}\ r(pt \pm \theta) \tag{8}$$

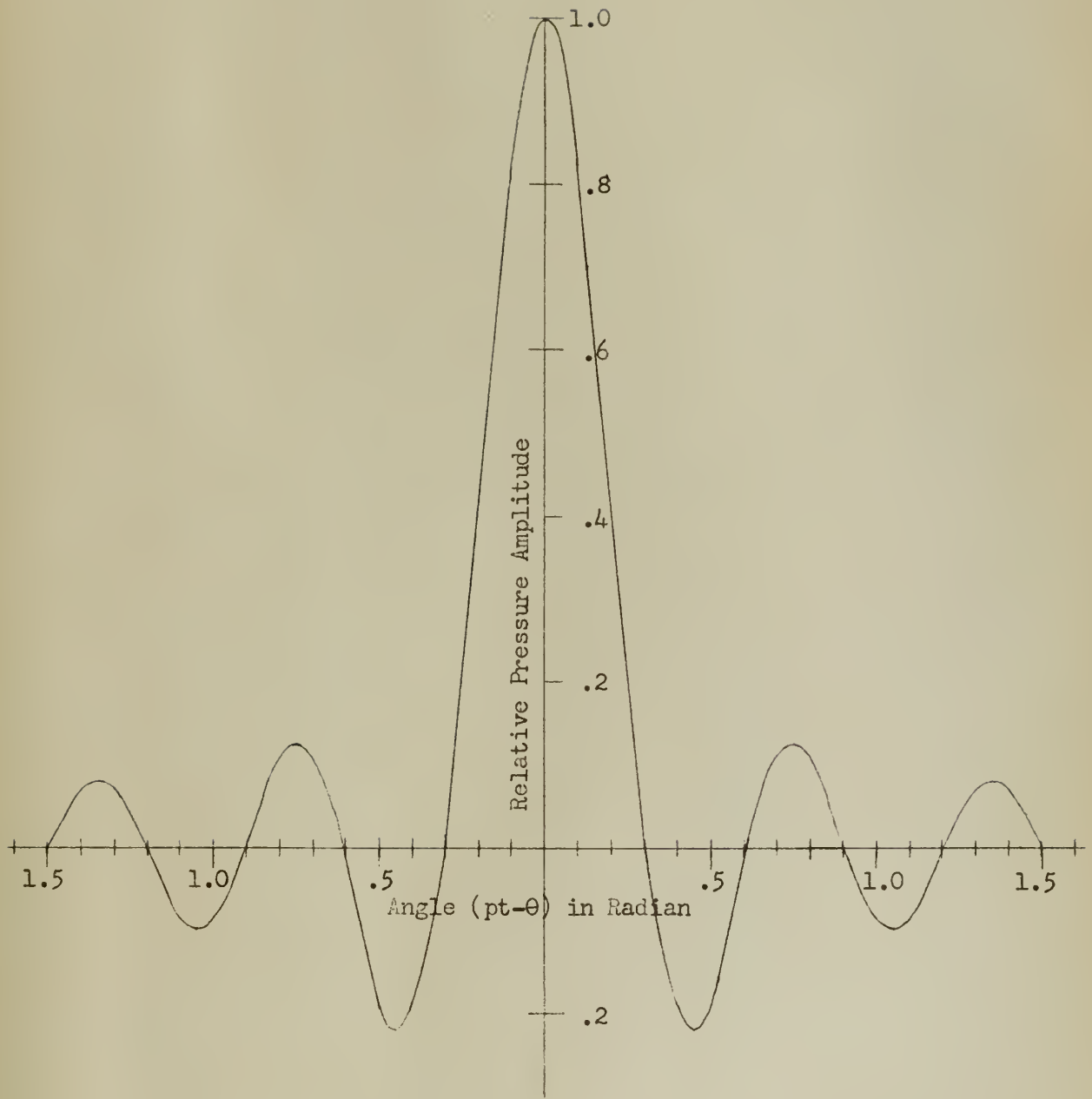

Figure 2. Plot of $P = 1 + 2 \sum_{r=1}^{10} \text{Cos } r(pt-\theta)$

This function is shown in Figure 2 for N = 10 (i. e. 21 section transducer) and can be seen to be a directivity pattern whose main lobe at any instant comes at an angular position determined by the position of the instant in the cycle of the frequency p. The process thus gives an angular scan of the available search sector, since the angular position θ is related to the angle of the incidence of signals on the hydrophone. The overall directivity of the system is, of course, Figure 2 (plotted against δ instead of θ) multiplied by the directivity of each individual hydrophone section. It may be stated, as a general rule, that the angle of scan is equal to the hydrophone beam width (3db) multiplied by the number of sections of the hydrophone.

Only one of the two signals contained in equation (7) is needed to give the scanned output, and the other is rejected by a filter.

Thesis
C668 Conable
Barium titanate sonar transducers.

32073